HHS Public Access

Author manuscript

*Cytoskeleton (Hoboken)*. Author manuscript; available in PMC 2015 June 29.

Published in final edited form as:

*Cytoskeleton (Hoboken)*. 2014 January ; 71(1): 61–78. doi:10.1002/cm.21159.

# CLIC5 Stabilizes Membrane-Actin Filament Linkages at the Base of Hair Cell Stereocilia in a Molecular Complex with Radixin, Taperin, and Myosin VI

**Felipe T. Salles**[1,†], **Leonardo R. Andrade**[1,†], **Soichi Tanda**[2,3,†], **M'hamed Grati**[1,†], **Kathleen L. Plona**[2], **Leona H. Gagnon**[4], **Kenneth R. Johnson**[4], **Bechara Kachar**[1], and **Mark A. Berryman**[3,5,*]

[1]Laboratory of Cell Structure and Dynamics, National Institute on Deafness and Other Communication Disorders, National Institutes of Health, Bethesda, Maryland [2]Department of Biological Sciences, Ohio University, Athens, Ohio [3]Interdisciplinary Program in Molecular & Cellular Biology, Ohio University, Athens, Ohio [4]The Jackson Laboratory, Bar Harbor, Maine [5]Department of Biomedical Sciences, Ohio University, Athens, Ohio

## Abstract

Chloride intracellular channel 5 protein (CLIC5) was originally isolated from microvilli in complex with actin binding proteins including ezrin, a member of the Ezrin-Radixin-Moesin (ERM) family of membrane-cytoskeletal linkers. CLIC5 concentrates at the base of hair cell stereocilia and is required for normal hearing and balance in mice, but its functional significance is poorly understood. This study investigated the role of CLIC5 in postnatal development and maintenance of hair bundles. Confocal and scanning electron microscopy of CLIC5-deficient jitterbug (*jbg*) mice revealed progressive fusion of stereocilia as early as postnatal day 10. Radixin (RDX), protein tyrosine phosphatase receptor Q (PTPRQ), and taperin (TPRN), deafness-associated proteins that also concentrate at the base of stereocilia, were mislocalized in fused stereocilia of *jbg* mice. TPRQ and RDX were dispersed even prior to stereocilia fusion. Biochemical assays showed interaction of CLIC5 with ERM proteins, TPRN, and possibly myosin VI (MYO6). In addition, CLIC5 and RDX failed to localize normally in fused stereocilia of MYO6 mutant mice. Based on these findings, we propose a model in which these proteins work together as a complex to stabilize linkages between the plasma membrane and subjacent actin cytoskeleton at the base of stereocilia.

[*]Address correspondence to: Mark A. Berryman, Department of Biomedical Sciences, Ohio University, Athens, Ohio. berryman@ohio.edu.

[†]F.T.S., L.R.A., S.T., and M.G. contributed equally to this work.

Felipe T. Salles's present address is Department of Otolaryngology, Stanford University School of Medicine, Stanford, CA, 94305.

Leonardo R. Andrade's present address is Institute of Biomedical Sciences, Federal University of Rio de Janeiro, Rio de Janeiro, RJ, Brazil, 21941-902.

M'hamed Grati's present address is Department of Otolaryngology, Laboratory of Human Molecular Genetics, University of Miami Miller School of Medicine, Miami, FL, 33136.

Kathleen L. Plona's present address is Medical Scientist Training Program, Case Western Reserve University, School of Medicine, Cleveland, OH 44106.



The authors declare no conflict of interest.

**Keywords**

chloride intracellular channel 5 (CLIC5); cytoskeleton; deafness; ezrin-radixin-moesin (ERM); hair cell; myosin VI (MYO6); PTPRQ; radixin; stereocilia; taperin

## Introduction

Hearing and balance rely on deflection of actin-based stereocilia bundles, mechanotransducers that convert mechanical stimuli into electric impulses transmitted to the brain. In the mammalian auditory system, the spiral cochlea houses the organ of Corti, an epithelial sheet comprised of a single row of inner hair cells and three rows of outer hair cells. Each hair cell displays a bundle of stereocilia on its apical surface, arranged in a staircase pattern with increasing heights. Hair bundles exhibit a continuous morphologic and tonotopic gradient along the cochlea; the shorter bundles responsive to high frequencies are found at the base, and the taller bundles responsive to low frequencies are found at the apex. In mice, bundles undergo a 2-week postnatal maturation process, growing in width and height to form a bundle of 3–4 rows at the onset of hearing [Lim and Anniko, 1985; Zuo, 2002].

Stereocilia are supported internally by tightly crosslinked parallel actin filaments of uniform polarity, with the barbed (plus) ends at the distal tips [Tilney et al., 1980]. Molecular-genetic studies have highlighted the functional significance of molecular compartmentalization within stereocilia [Frolenkov et al., 2004; Petit and Richardson, 2009; Schwander et al., 2010; Richardson et al., 2011]. Distinct protein complexes consisting of transmembrane proteins, submembranous scaffolding proteins, and myosin motors link to the actin core at specific sites, regulating processes such as bundle development, maintenance of the steady state [Schneider et al., 2002; Rzadzinska et al., 2004; Belyantseva et al., 2005] and mechanotransduction [Peng et al., 2011]. In addition to specific protein complexes that form specialized lateral attachments between adjacent ster-eocilia, such as tip links [Siemens et al., 2004; Ahmed et al., 2006; Alagramam et al., 2011; Caberlotto et al., 2011; Grati and Kachar, 2011], and ankle links [McGee et al., 2006; Michalski et al., 2007; Grati et al., 2012], there are also pronounced differences in plasma membrane lipid composition from proximal region to distal tip of stereocilia [Zhao et al., 2012]. At the proximal end, the shaft gradually narrows to form a conical taper through which a dense rootlet of actin filaments penetrates into the cuticular plate [Tilney et al., 1980], serving as the pivot point upon mechanical deflection of the stiff hair bundle [Crawford and Fettiplace, 1985; Karavitaki and Corey, 2010]. Stereocilia of mice carrying mutations in proteins that concentrate at the base of the hair bundle generally develop during embryogenesis but deteriorate postnatally [Self et al., 1999; Goodyear et al., 2003; Kitajiri et al., 2004]. Such proteins include myosin VI (MYO6), radixin (RDX), protein tyro-sine phosphatase receptor Q (PTPRQ), taperin (TPRN), and chloride intracellular channel 5 (CLIC5) [Goodyear and Richardson, 1992; Hasson et al., 1997; Pataky et al., 2004; Gagnon et al., 2006; Sakaguchi et al., 2008; Rehman et al., 2010]. However, the presence of a multiprotein complex in this taper region, and a more specific function of CLIC5 remain to be described.

Members of the chloride intracellular channel protein family (CLIC1–6), contrary to their name, have non-channel functions, and their N- and C-terminal halves share homology with thioredoxin/GST-N and GST-C family domains, respectively [Littler et al., 2010]. CLIC5 was originally isolated from microvilli of human placenta epithelium in a cytoskeletal protein complex containing F-actin and several actin-binding proteins including ezrin [Berryman and Bretscher, 2000; Berryman et al., 2004], an ERM protein that couples the plasma membrane to the actin cytoskeleton [Bretscher et al., 2000; Fehon et al., 2010]. CLIC5 has two isoforms generated by alternative splicing of the first exon: CLIC5A (251 residues), and CLIC5B (410 residues), which has a longer N-terminus [Shanks et al., 2002a]. CLIC5A is the predominant isoform expressed in hair bundles [Gagnon et al., 2006] and is hereafter referred to as CLIC5. Similar to RDX, CLIC5 concentrates at the proximal region of stereocilia in the bullfrog and mouse, and CLIC5-deficient (jitterbug, *jbg*) mice exhibit progressive hearing loss and vestibular dysfunction [Gagnon et al., 2006]. Within two weeks after birth, stereocilia of *jbg* mice begin to degenerate, eventually leading to loss of hair cells.

The goal of this study was to reveal functional roles for CLIC5 by uncovering new *jbg* phenotypes and protein interactions. Here, we present new evidence that CLIC5 plays a critical role in membrane-cytoskeletal attachment at the base of the hair bundle by interacting with several other proteins localized at the base of stereocilia: RDX, TPRN, and MYO6. These findings suggest the presence of a multi-protein complex that stabilizes linkages between the plasma membrane and subjacent actin filaments, crucial for maintaining the unique shape and functional properties of stereocilia.

## Results

### CLIC5 Deficiency Causes Defects in Bundle Organization in Postnatal *jbg* Mice

Given that CLIC5 is enriched at the base of stereocilia, we asked whether it generates a phenotype similar to knockout models of proteins localized to the same compartment, including RDX, MYO6, and PTPRQ by analyzing jitterbug (*jbg*) mice under scanning electron microscopy (SEM). At P2, hair bundle morphology in *jbg* mutant mice appeared normal throughout most of the cochlear duct (data not shown) as found in heterozygous mice (Fig. 1A). At later stages of maturation, defects in hair bundle morphology were readily apparent. At P17, inner hair cells at the apex of *jbg* cochleae displayed stereocilia that were fused (Fig. 1B, arrowhead) or even greatly enlarged in length and diameter (Fig. 1B, arrows). Heterozygous *jbg*/+ control hair cell stereocilia presented no morphological change at P17 (Fig. 1A). Mutant inner hair cells at the cochlear base displayed extensive stereocilia fusion (Fig. 1D, arrowheads) and membrane lifting (Fig. 1D, asterisks), distinct from their heterozygous littermates (Fig. 1C). Outer hair cells at the apex of *jbg* cochleae showed general bundle disorganization and missing stereocilia, particularly at the bundle vertex (data not shown). Loss of stereocilia at the bundle vertex could be observed by SEM and confocal microscopy of phalloidin-stained specimens, and was evident as early as P5 (data not shown). However, bundles viewed by SEM still displayed a staircase pattern. Mutant outer hair cells from the middle and base regions of the cochlear duct exhibited a more pronounced phenotype than those from the apex. At the very base, outer hair cell

bundles were mostly or entirely engulfed by the membrane (Fig. 1F). Cells from the middle region had a less severe phenotype, and generally exhibited fused or missing stereocilia and lifting of the apical membrane. Some cells displayed a pheno-type in which the membrane was lifted off an entire arm of the V-shaped bundle (Fig. 1G, arrows) and others showed fused stereocilia at the free ends of the arms (Fig. 1G, asterisks). Extensive membrane lifting and stereocilia fusion in outer hair cells was not apparent at P10 or P14 (data not shown), suggesting that onset of this phenotype in outer hair cells occurs around P15 or later. In contrast to outer hair cells, stereocilia of inner hair cells at the apex of the cochlea fused earlier, by P10 (Fig. 1B, inset, arrow), and bundle disorganization in these cells was observed by confocal microscopy as early as P5 (data not shown).

At the apex of P40 cochleae, all inner hair cells and the first row of outer hair cells consistently displayed bundle fusions; individual (unfused) stereocilia were still present in second and third row outer hair cells (data not shown). Vestibular hair cells of *jbg* mice (P17) also showed fused, thickened, and elongated stereocilia covered by the plasma membrane (Figs. 1I–1J), consistent with the described vestibular phenotype [Gagnon et al., 2006].

Taken together, these results indicated that CLIC5 plays a key role in the positioning and maintenance of stereocilia shape. The loss of stereocilia at the bundle vertex and the fusion of stereocilia in postnatal *jbg* mice was similar to what was observed in RDX [Kitajiri et al., 2004], PTPRQ [Goodyear et al., 2003; Sakaguchi et al., 2008], and MYO6 [Self et al., 1999] deficient mice.

## CLIC5 Localizes at the Base of Stereocilia in Developing and Mature Hair Cells

CLIC5 was previously localized to the base of stereocilia [Gagnon et al., 2006] using an affinity-purified antibody [Berryman and Bretscher, 2000]. However, heat-induced antigen retrieval was required to reveal masked epitopes. Given the potential for artifacts [D'Amico et al., 2009], we re-examined the localization of CLIC5 using light and electron microscopy.

First, we developed an independent affinity-purified antibody that recognizes a single band corresponding to the size of CLIC5 in mouse lung extract (Fig. 2). Still, no specific staining was observed in hair cells without antigen retrieval. Incubation in citrate buffer at 60°C for 30 min [Schneider et al., 2006] showed a consistent recovery of stereocilia immunoreactivity as early as P1 (data not shown) persisting through adulthood (Figs. 3A and 3B, arrows), as well as in microvilli, consistent with the previous descriptions [Berryman and Bretscher, 2000; Gagnon et al., 2006].

Second, we tested the ability of hair cells to sort and compartmentalize exogenously expressed CLIC5. Trans-fected rat vestibular hair cells showed a concentration gradient of an N-terminal GFP fusion construct (GFP-CLIC5) from the base to the tips of stereocilia (Fig. 3C and 3E) in 89.6% of transfected hair cells ($n$ = 29). This construct also localized to microvilli of transfected LLC-PK1-CL4 cells, which express little or no endogenous CLIC5 (Fig. 4). The GFP-CLIC5 fusion protein was also present to varying degrees of enrichment in the cytoplasm and nucleus of transfected cells; similar localization occurred with GFP fused to the C-terminus of CLIC5 (data not shown).

Third, we examined the localization of CLIC5 with both antibodies using post-embedding immunogold electron microscopy of rat tissue. The antibodies consistently labeled the base of the stereocilia as well as the apical plasma membrane between stereocilia, whereas gold particles were essentially excluded from the core actin rootlets projecting into the cuticular plate (Figs. 5A and 5B). The localization of CLIC5 to the apical inter-stereocilia membrane domain is similar to that of MYO6 in hair cells [Hasson et al., 1997] and brush border microvilli in intestinal epithelial cells [Hegan et al., 2012]. Together, these results firmly establish the localization of CLIC5 within the taper region at the base of stereocilia, and at the hair cell apical plasma membrane.

## CLIC5 is Required for Proper Compartmentalization of PTPRQ and RDX at the Base of Stereocilia

Next, we asked whether CLIC5 is required for proper localization of PTPRQ, RDX, and TPRN at the base of stereocilia. To better visualize the staining pattern along the proximal-to-distal axis of stereocilia, we compared inner hair cells near the apex of the cochlear duct, focusing primarily on the tallest row. Inner ear tissues were stained with affinity-purified antibodies against each protein at different developmental stages, ranging from P5 to P40 in control (*jbg*/+) and CLIC5-deficient (*jbg/jbg*) mice.

In mature hair cells, PTPRQ was well compartmentalized at the base of stereocilia (P40, Figs. 6A and 6C, arrow) and the apical membrane (Figs. 6A and 6C, arrowhead). However, in the *jbg* mutant the distribution of PTPRQ on the plasma membrane was drastically altered and appeared uniform in fused stereocilia at P40 (Figs. 6D and 6F, arrows). RDX was highly concentrated at the base of stereocilia and in microvilli of support cells in control animals. In P17 control hair cells, RDX was enriched at the base of stereocilia with relatively low levels along the shaft (Figs. 6G and 6I, arrows). In some mutant cells, RDX staining was dispersed along the entire shaft of stereocilia and individual actin bundles were still recognizable underneath the lifted plasma membrane (Figs. 6J and 6L, arrows). TPRN localized to the proximal end of stereocilia in control hair cells and also concentrated in microvilli of support cells. At P21, TPRN localization was confined to the base of control stereocilia (Figs. 6M and 6O, arrows); however, in mutant cells TPRN staining was punctuated and distributed throughout both fused (Figs. 6P and 6R, arrows) and unfused (Figs. 6P and 6R, arrowheads) stereocilia. These data suggest that CLIC5 may play a role in maintaining the localization of PTPRQ, RDX, and TPRN at the base of stereocilia after hair cells mature (P17).

Prior to hair cell maturation, at P10, PTPRQ was restricted to the base of stereocilia (Figs. 7A and 7C, arrows); however, this localization was altered in the *jbg* mutant even in cells where individual stereocilia were distinguishable (Figs. 7D and 7F, arrow). Localization of PTPRQ, although still stronger at the base, was not restricted to this compartment, but also was seen along the shaft of stereocilia (Figs. 7D and 7F, arrow). Similarly, at P7 RDX was more dispersed along the length of mutant (Figs. 7J and 7L, arrow) than control stereocilia (Figs. 7G and 7I, arrows). In contrast, TPRN localization at the base of stereocilia appeared similar between control (Figs. 7M and 7O, arrows) and mutant (Figs. 7P and 7R, arrows) inner hair cells; likewise, TPRN localization appeared normal in P5 mutant cells (data not

shown). The altered distributions of PTPRQ and RDX before completion of hair cell maturation in the mutant were confirmed by quantitative analyses of pixel intensity profiles taken from the base to the tip of stereocilia at P10 (Figs. 8). Together, these findings indicate that CLIC5 influences the proper localization of PTPRQ and RDX to the base of stereocilia during postnatal maturation of hair bundles.

### CLIC5 Interacts Biochemically with ERM Proteins and TPRN

Previous studies have shown that CLIC5 interacts with multiple proteins in distinct tissues and subcellular compartments. CLIC5 associates with actin, ezrin, a-actinin, gelsolin, and IQGAP1 in placental microvilli [Berryman and Bretscher, 2000; Berryman et al., 2004], with ezrin and podocalyxin in kidney podocyte processes [Pierchala et al., 2010; Wegner et al., 2010], and with AKAP350, a large scaffolding protein that concentrates at the centrosome and the Golgi apparatus [Shanks et al., 2002a,b]. Based on these findings, we hypothesized that CLIC5 might be part of a complex that connects the plasma membrane to the underlying actin cytoskeleton at the base of stereocilia, along with RDX, PTPRQ, and MYO6. We then examined physical interactions between CLIC5 and candidate interacting proteins by coimmunoprecipitation from transfected LLC-PK1-CL4 cells, which are known to abundantly express ezrin in microvilli [Crepaldi et al., 1997]. In transfected cells, GFP-CLIC5 localized to actin-rich microvilli (Fig. 4A–4C); on Western blots of SDS-soluble extracts, a ~60 kDa band corresponding to the expected size of the GFP-CLIC5 fusion protein was readily observed, but endogenous CLIC5 (~32 kDa) was not detectable (Fig. 4D). In anti-GFP immunoprecipitates, a band corresponding to the size of ezrin was detected (Fig. 9A). The use of a crosslinker (DSP) immediately before cell lysis [Viswanatha et al., 2012] greatly enhanced the amount of ezrin in the immunoprecipitate. The levels of ezrin were consistently ($n = 3$) weak relative to the amount of CLIC5 in the immunoprecipitates. One explanation for this result is that only a small fraction of overexpressed CLIC5 is associated with ezrin. Another possibility is that CLIC5 and ezrin may interact transiently. Our results are reminiscent of what has been shown previously for ezrin-NHERF1/EBP50 complexes, which are unstable in immunoprecipitates [Garbett and Bretscher, 2012].

A yeast 2-hybrid screen in which CLIC1 was used as bait identified a partial cDNA clone (IMAGE: 5804540) corresponding to a C-terminal fragment (amino acids 307–711) of TPRN [Lehner et al., 2004]. Moreover, we also identified TPRN as a partner for CLIC4 in a yeast 2-hybrid screen (M. Berryman, Ohio University, and W. Moolenaar, Netherlands Cancer Institute, unpublished data). To test for potential interaction between CLIC5 and TPRN, an Xpress epitope tag fused to the C-terminal 404 amino acids of human TPRN was expressed in LLC-PK1-CL4 epithelial cells, where it localized to the cytoplasm and nucleus (data not shown), consistent with previous findings [Ferrar et al., 2011]. Using crosslinking immunoprecipitation, we found that GFP-CLIC5 was present in Xpress-TPRN immunoprecipitates (Fig. 9B). Conversely, Xpress-TPRN was present in GFP immunoprecipitates (Fig. 9C).

Using an independent approach, we prepared fractions of mouse lung (Fig. 10) by differential centrifugation and detergent solubilization of pellets containing membrane and cytoskeletal elements (Fig. 10A). Immunoblotting of the various fractions showed that

CLIC5 was enriched in the detergent-insoluble membrane/cytoskeletal pellet and was resistant to detergent extraction, similar to a-actinin, b-actin (Fig. 10B), RDX, and ezrin; MYO6 was particularly recalcitrant to detergent extraction (Fig. 10C). Cytoskeletal pellets were treated with detergent and high salt to help break pre-existing protein-protein interactions, returned to physiological salt levels, and then incubated with affinity beads containing CLIC5 or control beads containing BSA or GST. Since CLIC proteins have structural homology to members of the GST superfamily [Dulhunty et al., 2001; Harrop et al., 2001], GST was used as a control for non-specific binding in addition to BSA. CLIC5 specifically bound to intact RDX (Fig. 10C, arrowhead) and ezrin. In blots probed with affinity-purified MYO6 antibody, a prominent band at ~200 kDa was seen along with a faster migrating immunoreactive band at ~160 kDa (Fig. 10C, asterisk). This faster migrating band is likely a degradation product, similar to what was previously observed in blots of isolated frog hair bundles [Hasson et al., 1997]. Both bands were resistant to extraction with detergent and high salt. The faster migrating band bound to CLIC5 but not GST or BSA, and was enriched by CLIC5 over the starting material compared with RDX and ezrin. The faster migrating band was also seen in the starting material; although the prominent ~200 kDa band was not detected in the starting material (Fig. 10C, lane S), a small amount of this band bound to CLIC5 (arrowhead). Together, the coimmunoprecipitation and pull-down assay provide evidence that CLIC5 can physically interact directly or indirectly with ezrin, RDX, TPRN, and possibly MYO6.

### MYO6 is Required for Localization of CLIC5 and RDX

Unlike all other unconventional myosins, MYO6 is a minusend directed motor that acts both as a transport molecule and as an anchoring element [Nambiar et al., 2010]. Previous studies demonstrated that mutations in PTPRQ, MYO6, and RDX result in fusion of stereocilia [Self et al., 1999; Goodyear et al., 2003; Kitajiri et al., 2004; Ahmed et al., 2006], and that the proper localization of PTPRQ is dependent on MYO6, suggesting the presence of a molecular complex [Sakaguchi et al., 2008]. Because CLIC5 is required for localization of PTPRQ and RDX (Figs. 6 and 7), and because our biochemical data suggest that MYO6 may interact directly or indirectly with CLIC5 (Fig. 10C), we examined the localization of CLIC5 and RDX in inner hair cells of Snell's waltzer 2 Jackson (*Myo6*$^{sv\text{-}2J}$) mice. In control cells, CLIC5 and RDX are concentrated at the base of stereocilia (Figs. 11A and 11B, arrows). However, in the *sv-2J* mutant, both proteins were distributed along the shaft of giant stereocilia that had fused and elongated (Figs. 11C and 11D, arrowheads). These findings are consistent with the hypothesis that MYO6 functions to maintain the localization of CLIC5 and RDX as well as PTPRQ at the base of the stereocilia.

## Discussion

CLIC5 deficiency in the *jbg* mouse reveals a critical role for this protein in postnatal maturation and maintenance of hair cell stereocilia. To this end, the localization of CLIC5 to the base of stereocilia together with the pronounced plasma membrane lifting and consequent fusion of stereocilia in *jbg* mice provide compelling evidence that CLIC5 plays a critical role in stabilizing membrane-cytoskeletal attachments at the base of the hair bundle, in concert with RDX, TPRN, PTPRQ, and MYO6.

### CLIC5 Stabilizes Membrane-Cytoskeletal Attachments at the Hair Bundle Base

The pronounced membrane lifting and fusion of stereocilia in CLIC5-deficient hair cells highlights the critical importance of a secure connection between the plasma membrane and the actin cytoskeleton at the base of the hair bundle. The stereocilia of *jbg* mice exhibit a normal morphological appearance for about a week after birth, suggesting that CLIC5 is not required for early maturation. However, fusion of stereocilia begins as early as postnatal day 10 (inner hair cells) and continues into adulthood, indicating that CLIC5 plays a role in later stages of bundle maturation as well as maintenance in the adult. The graded severity of fusion phenotypes from the base to the apex in both inner and outer hair cells could be related to the shorter lengths or the more advanced developmental stage of stereocilia at the cochlear base. The onset of fusions in *jbg* mice is earlier for inner (before P14) compared with outer (after P14) hair cells, and giant elongated stereocilia are observed exclusively in inner hair cells near the apex, possibly reflecting their different intrinsic functions. Giant stereocilia could arise because of a temporal requirement for CLIC5 specific to inner hair cells, perhaps relating to rates of protein synthesis or protein turnover during bundle maturation [Rzadzinska et al., 2004; Grati et al., 2006; Zhang et al., 2012]. For example, if membrane-cytoskeletal linkage between and within individual stereocilia is compromised around the time of elongation, then adjacent actin bundles may fuse together through crosslinkers such as espin [Zheng et al., 2000; Rzadzinska et al., 2005], and then continue to elongate. These longer fused stereocilia are also seen in *Myo6* mutants in both inner and outer hair cells, and they appear at an earlier age [Self et al., 1999; Hertzano et al., 2008] than we observed in the *jbg* mutant.

### CLIC5 Functions as Part of a Multiprotein Linker Complex

Our data lead to the hypothesis that CLIC5 is part of a protein complex required for stabilizing membrane-cytoskeletal linkages at the base of the hair bundle (Fig. 12). CLIC5 shares a compartment near the base of stereocilia [Gagnon et al., 2006] with RDX [Pataky et al., 2004], PTPRQ [Goodyear and Richardson, 1992; Sakaguchi et al., 2008], TPRN [Rehman et al., 2010], and MYO6 [Hasson et al., 1997; Sakaguchi et al., 2008]. Furthermore, deficiencies of MYO6 [Avraham et al., 1997; Melchionda et al., 2001; Ahmed et al., 2003; Mohiddin et al., 2004], RDX [Khan et al., 2007; Shearer et al., 2009; Lee et al., 2011], PTPRQ [Schraders et al., 2010; Shahin et al., 2010], TPRN [Li et al., 2010; Rehman et al., 2010], and CLIC5 [C. Zazo Seco, H. Kremer, M. Schraders, Radboud University Nijmegen Medical Centre, 2013, personal communication] are all linked to human deafness, underscoring the significance of this hypothetical protein complex.

Genetic evidence from mouse knockout models shows comparable bundle defects. Similar to *Clic5*$^{jbg}$, *Rdx* knockout mice exhibit loss of stereocilia at the vertex of the hair bundle in outer hair cells and stereocilia fusion in both inner and outer hair cells [Kitajiri et al., 2004]. *Ptprq* knockout mice show fusion and elongation of stereocilia in inner hair cells and shortened U-shaped bundles on outer hair cells [Goodyear et al., 2003]. Stereocilia fusion in both inner and outer hair cells is present in *Myo6* knockout mice, as well as abnormal bundle orientation [Self et al., 1999; Mochizuki et al., 2010]. The onset of fusion in *Myo6* mutants is the earliest (before P3) among the members of the putative protein complex reported to date, suggesting a central role for MYO6, the only molecular motor in this complex. Despite

being a robust membrane-cytoskeletal linker [Self et al., 1999; Hegan et al., 2012], MYO6 alone may be unable to provide sufficient anchorage at the base because loss of any other member of the proposed protein complex results in membrane lifting. This suggests an interdependent and dynamic functional relationship among PTPRQ, a transmembrane protein at the base of stereocilia [Goodyear and Richardson, 1992; Sakaguchi et al., 2008], CLIC5, and the membrane-cytoskeletal linkers MYO6 and RDX.

Another line of evidence to support our hypothesis is the finding that CLIC5 deficiency results in altered distributions of PTPRQ, RDX, and TPRN in fused stereocilia of *jbg* mice, similar to those for CLIC5 and RDX in the *Myo6* knockout. The dramatic redistribution of these proteins after stereocilia fusion in *Clic5*$^{jbg}$ and *Myo6* mutants is consistent with previous studies indicating a random diffusion of PTPRQ within the membrane of fused stereocilia in *Myo6* mutant hair cells [Sakaguchi et al., 2008]. Although we cannot rule out the possibility that one or more proteins may be mislocalized as a secondary consequence of stereocilia fusion, we observed perturbations in PTPRQ and RDX localization prior to stereocilia fusion in *jbg* mice. This may reflect an initial molecular defect that leads to membrane lifting, and indicates that compartmentalization of CLIC5 at the base of the hair bundle is critical to maintain the taper and prevent membrane lifting. Our observation that PTPRQ and RDX exhibit a more diffuse pattern but still with a base-to-tip gradient in hair bundles of *jbg* mice suggests that the localization of these proteins during bundle maturation is regulated not only by CLIC5 but also by other proteins such as MYO6. Conceivably, differences in localization of individual proteins could reflect differences in protein-protein interactions, or their dynamics at particular membrane microdomains having specific protein and lipid compositions [Zhao et al., 2012].

The compartmentalization of GFP-CLIC5 at the base of the hair bundle is compatible with a mechanism driven by actin filament minus end-directed MYO6 motor activity [Sakaguchi et al., 2008], comparable to tip protein compartmentalization by plus end-directed motors [Salles et al., 2009]. Biophysical studies show that MYO6 is an efficient transporter and also acts as a membrane-cytoskeletal linker [Chuan et al., 2011]. Thus, MYO6 may have dual functions by acting on one hand as a transporter to compartmentalize a protein complex at the base, and on the other hand as a linker to maintain mechanical tension by connecting actin filaments to the apical membrane. MYO6 alone is not sufficient to maintain stereocilia integrity in CLIC5- or RDX-deficient hair cells, which suggests that CLIC5 and RDX provide the necessary reinforcement.

Additional support for the presence of a protein complex comes from the coimmunoprecipitation and pull-down experiments showing that CLIC5 interacts physically with ezrin, RDX, TPRN, and possibly MYO6 as potential binding partners. ERM proteins are conformationally regulated by $PIP_2$-dependent phosphorylation that relieves an autoinhibitory intramolecular interaction between the membrane-binding N-domain and actin-binding C-domain [Fehon et al., 2010]. Membrane binding can be direct or indirect through PDZ scaffolding proteins NHERF1/EBP50 and NHERF2/E3KARP [Bretscher et al., 2000]. NHERF2 concentrates at the base of chick hair bundles and can potentially interact with multiple PDZ ligands involved in bundle assembly, structure, and function [Shin et al., 2013]. Proof of a direct interaction between CLIC5 and ERMs (or NHERF2) remains

elusive [Jiang et al., 2013], and chemical crosslinking enhances coimmunoprecipitation, suggesting that there may be a transient interaction such as the highly dynamic interaction between ezrin and NHERF1/EBP50 in microvilli [Garbett and Bretscher, 2012]. Our biochemical fractionation shows that CLIC5 is tightly associated with the cytoskeleton and resistant to detergent extraction in extracts of lung tissue, arguing in favor of a linker function, rather than an ion channel in hair cells. Previous studies show that CLIC5 binds to ezrin in kidney podocytes [Pierchala et al., 2010; Wegner et al., 2010], potentially connecting podocalyxin to the cytoskeleton. Although there is a lack of direct evidence at this time, an analogous linker complex may exist in the basal region of the hair bundle, wherein a CLIC5-RDX or CLIC5-RDX-NHERF1/EBP50 scaffold may connect PTPRQ or other membrane proteins to the cytoskeleton.

As a pivot point, the tapered base of the stereocilium is subjected to considerable mechanical stress. Outer hair cells, for example, undergo constant vibration producing forces in the nN range by outer hair cell electromotility [Mammano and Ashmore, 1993; Iwasa and Adachi, 1997; Frank et al., 1999]. Accordingly, extensive crosslinking of membrane proteins to the lateral surface of actin filaments would provide firm anchorage to counteract shear stresses at the base of the bundle. In addition, the tapered base is a site where the minus ends of peripheral actin filaments either terminate at the membrane in an orderly fashion [Tilney et al., 1980] or bend into the central rootlet [Furness et al., 2008], which extends into the subjacent cuticular plate and anchors to TRIOBP [Kitajiri et al., 2010]. Thus, proteins at the tapered base may also attach the minus ends of actin filaments to the membrane, condense actin filaments to form the central rootlet, and possibly regulate depolymerization during bundle maturation [Rzadzinska et al., 2004] or at steady state during adulthood [Zhang et al., 2012]. Our results demonstrate that CLIC5 functions in stabilizing membrane-cytoskeletal attachments at the base of the hair bundle and suggest that CLIC5 works in concert with RDX, PTPRQ, TPRN, and MYO6. We postulate that lifelong resilience of hair bundles, which can withstand upwards of 20,000 deflections per second, depends on the existence of specific protein complexes critical to the stability of this structurally and functionally important domain.

## Materials and Methods

### Animals

Colonies of CLIC5-deficient *jbg* mice (C3H/HeJ-*Clic5*$^{jbg}$/J) were maintained in animal facilities at NIH (NIDCD protocol 1215-05) and Ohio University (Institutional Animal Care and Use Committee protocol 12-H-029). Animals were genotyped by PCR as previously reported [Gagnon et al., 2006]. A colony of *Myo6* mutant *sv-2J* mice (B6.Cg-*Myo6*$^{sv\text{-}2J}$/J) was maintained in animal facilities at NIH (NIDCD protocol 1215-05). Euthanasia of mice and rats was performed in strict accordance with NIH guidelines.

### Antibodies and Constructs

A polyclonal rabbit antibody specific to CLIC5 (APB56) was raised against human CLIC5A fused to GST, cross-adsorbed against CLIC4, and affinity-purified as previously described [Berryman and Bretscher, 2000]. The specificity of the antibody was verified by Western

blot (Fig. 2). Other rabbit antibodies used were whole antisera against CLIC5A [Berryman and Bretscher, 2000], ezrin [Bretscher, 1989], a-actinin [Bretscher and Weber, 1978], GFP (ab290, Abcam, Cambridge, MA), and affinity-purified antibodies against radixin (R3653, Sigma, St. Louis, MO), PTPRQ (PB619), MYO6 (PB136) [Sakaguchi et al., 2008], and taperin (HPA020899, Sigma). The taperin antibody was validated previously [Rehman et al., 2010]. Mouse monoclonal antibodies used were against β-actin (AAN02, Cyto-skeleton, Inc., Denver, CO) and Xpress epitope (R910-25, Life Technologies, Grand Island, NY). To make the GFP-CLIC5A fusion protein, the entire open reading frame of CLIC5A was amplified by PCR from the corresponding cDNA template [Berryman and Bretscher, 2000] using the following primers: forward primer atgcctcgagACA-GACTCGGCGACAGCTAAC which adds a 5′ XhoI restriction site, and reverse primer atgcggatccTCAG-GATCGGCTGAGGCGTTTG which adds a 3′ BamHI restriction site. The PCR product was digested with XhoI and BamHI and subcloned into pEGFP-C3 (Clontech Laboratories, Mountain View, CA) digested with the same enzymes. An N-terminal Xpress epitope fused to the C-terminal 404 residues of taperin was generated by PCR amplification of a cDNA with a partial coding sequence for taperin (GenBank accession BC098411) using the following primers: forward primer ttggtaccaGAGACCATCCC CTTGGGGGACCT which adds a 5′ KpnI restriction site, and reverse primer cTCAGAAATACAGGGCTGGCTC GCTGCGGA. The PCR product was digested with KpnI and subcloned into pcDNA3.1/ HisA (Life Technologies) after digestion with KpnI and EcoRV.

## Electron Microscopy

For transmission electron microscopy, freshly dissected inner ear tissues harvested from adult rats were fixed in 4% formaldehyde, 0.5% glutaraldehyde in 0.1*M* phosphate buffer, pH 7.2, with 2 m*M* $CaCl_2$, glycerinated, plunged into liquid Freon 22, and promptly transferred to liquid nitrogen. Frozen samples were freeze substituted in 1.5% uranyl acetate in absolute methanol at −90°C for 24 h, infiltrated with Lowicryl HM-20 resin at −45°C, and polymerized with UV light. Ultrathin sections were subjected to antigen retrieval for 10 min in 0.1% sodium borohydride and 50 m*M* glycine in 50 m*M* Tris, pH 7.4, 140 m*M* NaCl, 0.1% Triton X-100 (TBST). Next, thin sections were blocked in 10% normal goat serum in TBST for 1 h, incubated with 10 μg/mL APB56 or APB132 monospecific CLIC5 antibody [Berryman and Bretscher, 2000] in normal goat serum/TBST for 2 h and rinsed with TBST. Gold-labeled anti-rabbit secondary antibodies were then incubated at 1 part 10% normal goat serum to 20 parts polyethylene glycol in TBST for 2 h, then washed in TBST and stained with 1% uranyl acetate for 20 min. Specimens were viewed and photographed at 80 kV with a JEOL 1010.

For SEM, inner ears were fixed with a mixture of 2.5% glutaraldehyde, 4% formaldehyde, 50 m*M* HEPES buffer (pH 7.2), 2 mM $CaCl_2$, 1 m*M* $MgCl_2$, and 140 m*M* NaCl for 2 h at room temperature. Inner ear sensory organs were fine dissected and processed by a modified OTOTO method [Waguespack et al., 2007]. Thiocarbohydrazide was substituted by 1% tannic acid, alternating incubations of 1% osmium tetroxide and 1% tannic acid for 1 h each [Webb et al., 2011]. Samples were dehydrated, critical-point dried (Bal-Tec CPD 030), coated with a 4 nm platinum layer (Balzers BAF 300) and observed in a SEM Hitachi S-4800, operated at 5 kV.

### Immunofluorescence

Immunolocalizations were performed on whole mount preparations of freshly dissected organ of Corti. Temporal bones were dissected from euthanized rats and mice, followed by gentle perfusion with 4% formaldehyde in phosphate buffered saline (PBS) through the round window and fixation in situ for 30 min at room temperature. Organ of Corti pieces were dissected in PBS, followed by permeabilization with either 0.2% Triton X-100/PBS for 10 min (PTPRQ) or 0.5% Triton X-100/PBS for 30 min. For CLIC5, tissue was treated with 0.1*M* sodium citrate (pH 7.0) for 30 min at 60°C in a glass vial and then rinsed with PBS. After blocking in 4% BSA/PBS overnight at 4°C, tissue was stained for 2 h in primary antibody diluted in 4% BSA/PBS, washed in PBS, then stained for 1 h in Alexa 488-conjugated secondary antibody (Invitrogen, Carlsbad, CA) and Alexa 546-conjugated phalloidin diluted in PBS. After washing in PBS, specimens were mounted with Prolong Gold anti-fade (Invitrogen). Images were acquired with either a Zeiss 510 confocal laser scanning microscope or a spinning disk confocal (PerkinElmer, Wellesley, MA) on a Nikon Eclipse microscope (Tokyo, Japan).

Quantification of fluorescence intensity was performed on stereocilia from the tallest row of inner hair cells near the apex of the cochlear duct. Measurements were made with the National Institutes of Health ImageJ software after intensity levels were adjusted with Adobe Photoshop. Intensity profiles of rectangles going from base to tip of 10 individual stereocilia per group of PTPRQ, RDX, and actin were obtained, values averaged, normalized and plotted against stereocilia length using Microsoft Excel.

### Inner Ear Tissue Culture and Transfection

After $CO_2$ anesthesia, postnatal day 3–5 rat pups were euthanized, and their temporal bones were isolated and placed in L-15 medium (Invitrogen). Tissue explants were dissected and attached to coverslips previously coated with 150 g/L Cell Tak (BD Biosciences, San Jose, CA) as described previously [Rzadzinska et al., 2004]. Cultures were maintained in DMEM/F-12 (Invitrogen) supplemented with 5–7% fetal bovine serum (FBS) (Invitrogen) and 1.5 mg/mL ampicillin and kept at 37°C with 5% $CO_2$. Plasmid DNA (50 μg) was precipitated onto 25 mg of 1 μm gold particles and loaded into cartridges following the Helios Gene Gun protocol (Bio-Rad, Hercules, CA). Tissues were transfected with gold carriers at 95 psi helium pressure and incubated up to 48 h. Samples were washed briefly with PBS, fixed 30 min in 4% formaldehyde/PBS, permeabilized with 0.5% Triton X-100 in PBS containing Alexa Fluor 568-phalloidin for 30 min, washed, and mounted with Prolong anti-fade medium.

### Cell Culture and Transfection

LLC-PK1-CL4 epithelial cells were cultured as previously described [Zheng et al. 2010]. Cells grown on plastic culture dishes or glass coverslips were transfected with plasmid DNA using polyethylenimine (Polysciences, Inc. Warrington, PA) as previously described [Boussif et al., 1995]. Cells were processed for biochemistry or immunofluorescence within 12–21 h after addition of DNA. For immunofluorescence, cells were fixed with 4% formaldehyde/PBS for 10 min, permeabilized with 0.1% Triton X-100 for 60 s, and then processed for immunostaining.

## Immunoprecipitation

Crosslinking immunoprecipitation was performed using slight modifications of previously published procedures [Viswanatha et al., 2012]. A working stock of DSP (Dithio-bis[succinimidyl propionate], Thermo Fisher Scientific, Rockford, IL) was freshly prepared to 100 m*M* by dissolving in dimethylformamide (DMF). Cells grown in 100 mm dishes were rinsed briefly with PBS, incubated 2 min room temperature with 1 m*M* DSP/PBS or DMF/PBS as a control. Cells were rinsed briefly with 50 m*M* Tris, pH 7.4, 150 m*M* NaCl (TBS), followed by 2 min incubation in fresh ice-cold TBS. Cells were scraped in cold RIPA lysis buffer (0.1% SDS, 1% Triton X-100, 1% deoxycholate, 0.9% NaCl, 1 *mM* EDTA, 25 m*M* Tris, pH 7.4) containing phenylmethylsulfonyl fluoride, benzamidine, and Halt (Thermo Fisher Scientific) protease inhibitor cocktail, triturated, and ultracentrifuged 20 min at 100,000 × *g*. Samples of supernatants were prepared with SDS under reducing and non-reducing conditions to assess effects of crosslinking on bands of interest. Supernatants were incubated with protein-A or protein-G Sepharose (Sigma) and appropriate experimental and control antibodies. After extensive washing with RIPA buffer, proteins were eluted from beads by boiling in SDS sample buffer containing 5% 2-mercaptoethanol [Laemmli, 1970].

## Pull-Down Assay

Frozen mouse lungs were homogenized with a Waring blender in 10 vol (g/mL) ice cold homogenization buffer (20 m*M* HEPES, pH 7.4, 0.25*M* sucrose, 5 m*M* EDTA, 2 m*M* dithiothreitol), containing protease inhibitors . A starting homogenate was made on ice using a motor-driven Teflon pestle, followed by sequential passage through a 1000-mesh nylon screen and a double tea sieve. Unbroken cells and large organelles were removed by centrifugation 10 min at 900 × *g*. The volume of the supernatant was adjusted to the original volume of the starting homogenate, followed by ultracentrifugation 90 min at 100,000 × *g* to pellet membranes and cytoskeleton. The resulting pellet was resuspended in 1/10 volume of starting homogenate using 2% Triton X-100 in homogenization buffer containing protease inhibitors and incubated 10 min on ice. The sample was ultracentrifuged 15 min at 200,000 × *g* to pellet detergent-insoluble cytoskeletal residue. The supernatant was adjusted to 1.5*M* KCl and incubated on ice 20 min to facilitate disruption of protein interactions, followed by dilution with 10 vol cold 20 m*M* HEPES, pH 7.4, 0.2% Triton X-100, 2 m*M* DTT, and protease inhibitors. Equal volumes of this starting extract were added to equal volumes of affinity resin containing either purified 6×His-CLIC5A [Berryman and Bretscher, 2000], glutathione-S-transferase (*Shistosoma japonicum* GST, GE Healthcare, Piscataway, NJ) or BSA (Fraction V, Sigma). The affinity resins (cyanogen bromide-activated Sepharose, GE Healthcare) were prepared according to manufacturer's instructions using 4 mg protein per ml resin. After incubation with starting extract for 20 min at 4°C, beads were washed extensively with homogenization buffer and eluted with SDS sample buffer containing 5% 2-mercaptoethanol.

## Immunoblotting

Samples were separated on SDS-PAGE [Laemmli, 1970] and transferred to Immobilon P (EMD Millipore, Billerica, MA). Membranes were blocked with either 5% non-fat dry milk

or 5% BSA in TBS containing 0.1% Tween 20, and then probed with primary antibodies and peroxidase conjugated secondary reagents in the presence of 1% blocking agent. Bands were detected by enhanced chemiluminescence (EMD Millipore) and recorded on film or with a ChemiDoc XRS+ imaging system (Bio-Rad).

## Acknowledgments

The authors thank Kira Slepchenko for technical assistance, Danette Pratt for assistance with graphic art, Dr. Anthony Bretscher (Cornell University) for generous gifts of antibodies, Dr. James Bartles (Northwestern University) for LLC-PK1-CL4 cells, and Dr. Anthony Peng and Dr. Janet Duerr for helpful comments on the manuscript. M.A.B. and S. T. received financial support from Ohio University Heritage College of Osteopathic Medicine. K.R.J. and L.H.G. were supported by National Institutes of Health grant DC004301.

## References

Ahmed ZM, Morell RJ, Riazuddin S, Gropman A, Shaukat S, Ahmad MM, Mohiddin SA, Fananapazir L, Caruso RC, Husnain T, et al. Mutations of MYO6 are associated with recessive deafness, DFNB37. Am J Hum Genet. 2003; 72:1315–1322. [PubMed: 12687499]

Ahmed ZM, Goodyear R, Riazuddin S, Lagziel A, Legan PK, Behra M, Burgess SM, Lilley KS, Wilcox ER, Griffith AJ, et al. The tip-link antigen, a protein associated with the transduction complex of sensory hair cells, is protocadherin-15. J Neurosci. 2006; 26:7022–7034. [PubMed: 16807332]

Alagramam KN, Goodyear RJ, Geng R, Furness DN, van Aken AF, Marcotti W, Kros CJ, Richardson GP. Mutations in protocadherin 15 and cadherin 23 affect tip links and mechanotransduction in mammalian sensory hair cells. PLoS One. 2011; 6:e19183. [PubMed: 21532990]

Avraham KB, Hasson T, Sobe T, Balsara B, Testa JR, Skvorak AB, Morton CC, Copeland NG, Jenkins NA. Characterization of unconventional MYO6, the human homologue of the gene responsible for deafness in Snell's waltzer mice. Hum Mol Genet. 1997; 6:1225–1231. [PubMed: 9259267]

Belyantseva IA, Boger ET, Naz S, Frolenkov GI, Sellers JR, Ahmed ZM, Griffith AJ, Friedman TB. Myosin-XVa is required for tip localization of whirlin and differential elongation of hair-cell stereocilia. Nat Cell Biol. 2005; 7:148–156. [PubMed: 15654330]

Berryman M, Bretscher A. Identification of a novel member of the chloride intracellular channel gene family (CLIC5) that associates with the actin cytoskeleton of placental microvilli. Mol Biol Cell. 2000; 11:1509–1521. [PubMed: 10793131]

Berryman M, Bruno J, Price J, Edwards JC. CLIC-5A functions as a chloride channel in vitro and associates with the cortical actin cytoskeleton in vitro and in vivo. J Biol Chem. 2004; 279:34794–34801. [PubMed: 15184393]

Boussif O, Lezoualc'h F, Zanta MA, Mergny MD, Scherman D, Demeneix B, Behr JP. A versatile vector for gene and oligonucleotide transfer into cells in culture and in vivo: polyethylenimine. Proc Natl Acad Sci U S A. 1995; 92:7297–7301. [PubMed: 7638184]

Bretscher A. Rapid phosphorylation and reorganization of ezrin and spectrin accompany morphological changes induced in A-431 cells by epidermal growth factor. J Cell Biol. 1989; 108:921–930. [PubMed: 2646308]

Bretscher A, Weber K. Localization of actin and microfilament-associated proteins in the microvilli and terminal web of the intestinal brush border by immunofluorescence microscopy. J Cell Biol. 1978; 79:839–845. [PubMed: 365871]

Bretscher A, Chambers D, Nguyen R, Reczek D. ERM-Merlin and EBP50 protein families in plasma membrane organization and function. Annu Rev Cell Dev Biol. 2000; 16:113–143. [PubMed: 11031232]

Caberlotto E, Michel V, Foucher I, Bahloul A, Goodyear RJ, Pepermans E, Michalski N, Perfettini I, Alegria-Prevot O, Chardenoux S, et al. Usher type 1G protein sans is a critical component of the tip-link complex, a structure controlling actin polymerization in stereocilia. Proc Natl Acad Sci U S A. 2011; 108:5825–5830. [PubMed: 21436032]

Chuan P, Spudich JA, Dunn AR. Robust mechanosensing and tension generation by myosin VI. J Mol Biol. 2011; 405:105–112. [PubMed: 20970430]

Crawford AC, Fettiplace R. The mechanical properties of ciliary bundles of turtle cochlear hair cells. J Physiol. 1985; 364:359–379. [PubMed: 4032304]

Crepaldi T, Gautreau A, Comoglio PM, Louvard D, Arpin M. Ezrin is an effector of hepatocyte growth factor-mediated migration and morphogenesis in epithelial cells. J Cell Biol. 1997; 138:423–434. [PubMed: 9230083]

D'Amico F, Skarmoutsou E, Stivala F. State of the art in antigen retrieval for immunohistochemistry. J Immunol Methods. 2009; 341:1–18. [PubMed: 19063895]

Dulhunty A, Gage P, Curtis S, Chelvanayagam G, Board P. The glutathione transferase structural family includes a nuclear chloride channel and a ryanodine receptor calcium release channel modulator. J Biol Chem. 2001; 276:3319–3323. [PubMed: 11035031]

Fehon RG, McClatchey AI, Bretscher A. Organizing the cell cortex: the role of ERM proteins. Nat Rev Mol Cell Biol. 2010; 11:276–287. [PubMed: 20308985]

Ferrar T, Chamousset D, De Wever V, Nimick M, Andersen J, Trinkle-Mulcahy L, Moorhead GB. Taperin (c9orf75), a mutated gene in nonsyndromic deafness, encodes a vertebrate specific, nuclear localized protein phosphatase one alpha (PP1alpha) docking protein. Biol Open. 2011; 1:128–139. [PubMed: 23213405]

Frank G, Hemmert W, Gummer AW. Limiting dynamics of high-frequency electromechanical transduction of outer hair cells. Proc Natl Acad Sci U S A. 1999; 96:4420–4425. [PubMed: 10200277]

Frolenkov GI, Belyantseva IA, Friedman TB, Griffith AJ. Genetic insights into the morphogenesis of inner ear hair cells. Nat Rev Genet. 2004; 5:489–498. [PubMed: 15211351]

Furness DN, Mahendrasingam S, Ohashi M, Fettiplace R, Hackney CM. The dimensions and composition of stereociliary rootlets in mammalian cochlear hair cells: comparison between high- and low-frequency cells and evidence for a connection to the lateral membrane. J Neurosci. 2008; 28:6342–6353. [PubMed: 18562604]

Gagnon LH, Longo-Guess CM, Berryman M, Shin JB, Saylor KW, Yu H, Gillespie PG, Johnson KR. The chloride intracellular channel protein CLIC5 is expressed at high levels in hair cell stereocilia and is essential for normal inner ear function. J Neurosci. 2006; 26:10188–10198. [PubMed: 17021174]

Garbett D, Bretscher A. PDZ interactions regulate rapid turnover of the scaffolding protein EBP50 in microvilli. J Cell Biol. 2012; 198:195–203. [PubMed: 22801783]

Goodyear R, Richardson G. Distribution of the 275 kD hair cell antigen and cell surface specialisations on auditory and vestibular hair bundles in the chicken inner ear. J Comp Neurol. 1992; 325:243–256. [PubMed: 1281174]

Goodyear RJ, Legan PK, Wright MB, Marcotti W, Oganesian A, Coats SA, Booth CJ, Kros CJ, Seifert RA, Bowen-Pope DF, et al. A receptor-like inositol lipid phosphatase is required for the maturation of developing cochlear hair bundles. J Neurosci. 2003; 23:9208–9219. [PubMed: 14534255]

Grati M, Kachar B. Myosin VIIa and sans localization at stereocilia upper tip-link density implicates these Usher syndrome proteins in mechanotransduction. Proc Natl Acad Sci U S A. 2011; 108:11476–11481. [PubMed: 21709241]

Grati M, Schneider ME, Lipkow K, Strehler EE, Wenthold RJ, Kachar B. Rapid turnover of stereocilia membrane proteins: evidence from the trafficking and mobility of plasma membrane Ca(2+)-ATPase 2. J Neurosci. 2006; 26:6386–6395. [PubMed: 16763047]

Grati M, Shin JB, Weston MD, Green J, Bhat MA, Gillespie PG, Kachar B. Localization of PDZD7 to the stereocilia ankle-link associates this scaffolding protein with the Usher syndrome protein network. J Neurosci. 2012; 32:14288–14293. [PubMed: 23055499]

Harrop SJ, DeMaere MZ, Fairlie WD, Reztsova T, Valenzuela SM, Mazzanti M, Tonini R, Qiu MR, Jankova L, Warton K, et al. Crystal structure of a soluble form of the intracellular chloride ion channel CLIC1 (NCC27) at 1.4-A resolution. J Biol Chem. 2001; 276:44993–5000. [PubMed: 11551966]

Hasson T, Gillespie PG, Garcia JA, MacDonald RB, Zhao Y, Yee AG, Mooseker MS, Corey DP. Unconventional myosins in inner-ear sensory epithelia. J Cell Biol. 1997; 137:1287–1307. [PubMed: 9182663]

Hegan PS, Giral H, Levi M, Mooseker MS. Myosin VI is required for maintenance of brush border structure, composition, and membrane trafficking functions in the intestinal epithelial cell. Cytoskeleton (Hoboken). 2012; 69:235–251. [PubMed: 22328452]

Hertzano R, Shalit E, Rzadzinska AK, Dror AA, Song L, Ron U, Tan JT, Shitrit AS, Fuchs H, Hasson T, et al. A Myo6 mutation destroys coordination between the myosin heads, revealing new functions of myosin VI in the stereocilia of mammalian inner ear hair cells. PLoS Genet. 2008; 4:e1000207. [PubMed: 18833301]

Iwasa KH, Adachi M. Force generation in the outer hair cell of the cochlea. Biophys J. 1997; 73:546–555. [PubMed: 9199816]

Jiang L, Phang JM, Yu J, Harrop SJ, Sokolova AV, Duff AP, Wilk KE, Alkhamici H, Breit SN, Valenzuela SM, et al. CLIC proteins, ezrin, radixin, moesin and the coupling of membranes to the actin cytoskeleton: A smoking gun? Biochim Biophys Acta. 2013; 1828:134–146. [PubMed: 22659675]

Karavitaki KD, Corey DP. Sliding adhesion confers coherent motion to hair cell stereocilia and parallel gating to transduction channels. J Neurosci. 2010; 30:9051–9063. [PubMed: 20610739]

Khan SY, Ahmed ZM, Shabbir MI, Kitajiri S, Kalsoom S, Tasneem S, Shayiq S, Ramesh A, Srisailpathy S, Khan SN, et al. Mutations of the RDX gene cause nonsyndromic hearing loss at the DFNB24 locus. Hum Mutat. 2007; 28:417–423. [PubMed: 17226784]

Kitajiri S, Fukumoto K, Hata M, Sasaki H, Katsuno T, Nakagawa T, Ito J, Tsukita S. Radixin deficiency causes deafness associated with progressive degeneration of cochlear stereocilia. J Cell Biol. 2004; 166:559–570. [PubMed: 15314067]

Kitajiri S, Sakamoto T, Belyantseva IA, Goodyear RJ, Stepanyan R, Fujiwara I, Bird JE, Riazuddin S, Ahmed ZM, Hinshaw JE, et al. Actin-bundling protein TRIOBP forms resilient rootlets of hair cell stereocilia essential for hearing. Cell. 2010; 141:786–798. [PubMed: 20510926]

Laemmli UK. Cleavage of structural proteins during the assembly of the head of bacteriophage T4. Nature. 1970; 227:680–685. [PubMed: 5432063]

Lai NS, Wang TF, Wang SL, Chen CY, Yen JY, Huang HL, Li C, Huang KY, Liu SQ, Lin TH, et al. Phostensin caps to the pointed end of actin filaments and modulates actin dynamics. Biochem Biophys Res Commun. 2009; 387:676–681. [PubMed: 19622346]

Lee K, Amin Ud Din M, Ansar M, Santos-Cortez RL, Ahmad W, Leal SM. Autosomal Recessive nonsyndromic hearing impairment due to a novel deletion in the RDX Gene. Genet Res Int. 2011; 2011:294675. [PubMed: 22567349]

Lehner B, Semple JI, Brown SE, Counsell D, Campbell RD, Sanderson CM. Analysis of a high-throughput yeast two-hybrid system and its use to predict the function of intracellular proteins encoded within the human MHC class III region. Genomics. 2004; 83:153–167. [PubMed: 14667819]

Li Y, Pohl E, Boulouiz R, Schraders M, Nurnberg G, Charif M, Admiraal RJ, von Ameln S, Baessmann I, Kandil M, et al. Mutations in TPRN cause a progressive form of autosomal-recessive nonsyndromic hearing loss. Am J Hum Genet. 2010; 86:479–484. [PubMed: 20170898]

Lim DJ, Anniko M. Developmental morphology of the mouse inner ear. A scanning electron microscopic observation. Acta Otolaryngol Suppl. 1985; 422:1–69. [PubMed: 3877398]

Littler DR, Harrop SJ, Goodchild SC, Phang JM, Mynott AV, Jiang L, Valenzuela SM, Mazzanti M, Brown LJ, Breit SN, et al. The enigma of the CLIC proteins: ion channels, redox proteins, enzymes, scaffolding proteins? FEBS Lett. 2010; 584:2093–2101. [PubMed: 20085760]

Mammano F, Ashmore JF. Reverse transduction measured in the isolated cochlea by laser Michelson interferometry. Nature. 1993; 365:838–841. [PubMed: 8413667]

McGee J, Goodyear RJ, McMillan DR, Stauffer EA, Holt JR, Locke KG, Birch DG, Legan PK, White PC, Walsh EJ, et al. The very large G-protein-coupled receptor VLGR1: a component of the ankle link complex required for the normal development of auditory hair bundles. J Neurosci. 2006; 26:6543–6553. [PubMed: 16775142]

Melchionda S, Ahituv N, Bisceglia L, Sobe T, Glaser F, Rabionet R, Arbones ML, Notarangelo A, Di Iorio E, Carella M, et al. MYO6, the human homologue of the gene responsible for deafness in Snell's waltzer mice, is mutated in autosomal dominant nonsyndromic hearing loss. Am J Hum Genet. 2001; 69:635–640. [PubMed: 11468689]

Michalski N, Michel V, Bahloul A, Lefevre G, Barral J, Yagi H, Chardenoux S, Weil D, Martin P, Hardelin JP, et al. Molecular characterization of the ankle-link complex in cochlear hair cells and its role in the hair bundle functioning. J Neurosci. 2007; 27:6478–6488. [PubMed: 17567809]

Mochizuki E, Okumura K, Ishikawa M, Yoshimoto S, Yamaguchi J, Seki Y, Wada K, Yokohama M, Ushiki T, Tokano H, et al. Phenotypic and expression analysis of a novel spontaneous myosin VI null mutant mouse. Exp Anim. 2010; 59:57–71. [PubMed: 20224170]

Mohiddin SA, Ahmed ZM, Griffith AJ, Tripodi D, Friedman TB, Fananapazir L, Morell RJ. Novel association of hypertrophic cardiomyopathy, sensorineural deafness, and a mutation in unconventional myosin VI (MYO6). J Med Genet. 2004; 41:309–314. [PubMed: 15060111]

Nambiar R, McConnell RE, Tyska MJ. Myosin motor function: the ins and outs of actin-based membrane protrusions. Cell Mol Life Sci. 2010; 67:1239–1254. [PubMed: 20107861]

Pataky F, Pironkova R, Hudspeth AJ. Radixin is a constituent of stereocilia in hair cells. Proc Natl Acad Sci U S A. 2004; 101:2601–2606. [PubMed: 14983055]

Peng AW, Salles FT, Pan B, Ricci AJ. Integrating the biophysical and molecular mechanisms of auditory hair cell mechano-transduction. Nat Commun. 2011; 2:523. [PubMed: 22045002]

Petit C, Richardson GP. Linking genes underlying deafness to hair-bundle development and function. Nat Neurosci. 2009; 12:703–710. [PubMed: 19471269]

Pierchala BA, Munoz MR, Tsui CC. Proteomic analysis of the slit diaphragm complex: CLIC5 is a protein critical for podocyte morphology and function. Kidney Int. 2010; 78:868–882. [PubMed: 20664558]

Rehman AU, Morell RJ, Belyantseva IA, Khan SY, Boger ET, Shahzad M, Ahmed ZM, Riazuddin S, Khan SN, Friedman TB. Targeted capture and next-generation sequencing identifies C9orf75, encoding taperin, as the mutated gene in nonsyndromic deafness DFNB79. Am J Hum Genet. 2010; 86:378–388. [PubMed: 20170899]

Richardson GP, de Monvel JB, Petit C. How the genetics of deafness illuminates auditory physiology. Annu Rev Physiol. 2011; 73:311–334. [PubMed: 21073336]

Rzadzinska AK, Schneider ME, Davies C, Riordan GP, Kachar B. An actin molecular treadmill and myosins maintain stereocilia functional architecture and self-renewal. J Cell Biol. 2004; 164:887–897. [PubMed: 15024034]

Rzadzinska A, Schneider M, Noben-Trauth K, Bartles JR, Kachar B. Balanced levels of Espin are critical for stereociliary growth and length maintenance. Cell Motil Cytoskeleton. 2005; 62:157–165. [PubMed: 16206170]

Sakaguchi H, Tokita J, Naoz M, Bowen-Pope D, Gov NS, Kachar B. Dynamic compartmentalization of protein tyrosine phosphatase receptor Q at the proximal end of stereocilia: implication of myosin VI-based transport. Cell Motil Cytoskeleton. 2008; 65:528–538. [PubMed: 18412156]

Salles FT, Merritt RC Jr, Manor U, Dougherty GW, Sousa AD, Moore JE, Yengo CM, Dose AC, Kachar B. Myosin IIIa boosts elongation of stereocilia by transporting espin 1 to the plus ends of actin filaments. Nat Cell Biol. 2009; 11:443–450. [PubMed: 19287378]

Schneider ME, Belyantseva IA, Azevedo RB, Kachar B. Rapid renewal of auditory hair bundles. Nature. 2002; 418:837–838. [PubMed: 12192399]

Schneider ME, Dose AC, Salles FT, Chang W, Erickson FL, Burnside B, Kachar B. A new compartment at stereocilia tips defined by spatial and temporal patterns of myosin IIIa expression. J Neurosci. 2006; 26:10243–10252. [PubMed: 17021180]

Schraders M, Oostrik J, Huygen PL, Strom TM, van Wijk E, Kunst HP, Hoefsloot LH, Cremers CW, Admiraal RJ, Kremer H. Mutations in PTPRQ are a cause of autosomal-recessive nonsyndromic hearing impairment DFNB84 and associated with vestibular dysfunction. Am J Hum Genet. 2010; 86:604–610. [PubMed: 20346435]

Schwander M, Kachar B, Muller U. Review series: the cell biology of hearing. J Cell Biol. 2010; 190:9–20. [PubMed: 20624897]

Self T, Sobe T, Copeland NG, Jenkins NA, Avraham KB, Steel KP. Role of myosin VI in the differentiation of cochlear hair cells. Dev Biol. 1999; 214:331–341. [PubMed: 10525338]

Shahin H, Rahil M, Abu Rayan A, Avraham KB, King MC, Kanaan M, Walsh T. Nonsense mutation of the stereociliar membrane protein gene PTPRQ in human hearing loss DFNB84. J Med Genet. 2010; 47:643–645. [PubMed: 20472657]

Shanks RA, Larocca MC, Berryman M, Edwards JC, Urushidani T, Navarre J, Goldenring JR. AKAP350 at the Golgi apparatus. II. Association of AKAP350 with a novel chloride intracellular channel (CLIC) family member. J Biol Chem. 2002a; 277:40973–40980. [PubMed: 12163479]

Shanks RA, Steadman BT, Schmidt PH, Goldenring JR. AKAP350 at the Golgi apparatus. I. Identification of a distinct Golgi apparatus targeting motif in AKAP350. J Biol Chem. 2002b; 277:40967–40972. [PubMed: 12163481]

Shearer AE, Hildebrand MS, Bromhead CJ, Kahrizi K, Webster JA, Azadeh B, Kimberling WJ, Anousheh A, Nazeri A, Stephan D, et al. A novel splice site mutation in the RDX gene causes DFNB24 hearing loss in an Iranian family. Am J Med Genet A. 2009; 149A:555–558. [PubMed: 19215054]

Shin JB, Krey JF, Hassan A, Metlagel Z, Tauscher AN, Pagana JM, Sherman NE, Jeffery ED, Spinelli KJ, Zhao H, et al. Molecular architecture of the chick vestibular hair bundle. Nat Neurosci. 2013; 16:365–374. [PubMed: 23334578]

Siemens J, Lillo C, Dumont RA, Reynolds A, Williams DS, Gillespie PG, Muller U. Cadherin 23 is a component of the tip link in hair-cell stereocilia. Nature. 2004; 428:950–955. [PubMed: 15057245]

Tilney LG, Derosier DJ, Mulroy MJ. The organization of actin filaments in the stereocilia of cochlear hair cells. J Cell Biol. 1980; 86:244–259. [PubMed: 6893452]

Viswanatha R, Ohouo PY, Smolka MB, Bretscher A. Local phosphocycling mediated by LOK/SLK restricts ezrin function to the apical aspect of epithelial cells. J Cell Biol. 2012; 199:969–984. [PubMed: 23209304]

Waguespack J, Salles FT, Kachar B, Ricci AJ. Stepwise morphological and functional maturation of mechanotransduction in rat outer hair cells. J Neurosci. 2007; 27:13890–13902. [PubMed: 18077701]

Wang TF, Lai NS, Huang KY, Huang HL, Lu MC, Lin YS, Chen CY, Liu SQ, Lin TH, Huang HB. Identification and characterization of the actin-binding motif of phostensin. Int J Mol Sci. 2012; 13:15967–15982. [PubMed: 23443105]

Webb SW, Grillet N, Andrade LR, Xiong W, Swarthout L, Della Santina CC, Kachar B, Muller U. Regulation of PCDH15 function in mechanosensory hair cells by alternative splicing of the cytoplasmic domain. Development. 2011; 138:1607–1617. [PubMed: 21427143]

Wegner B, Al-Momany A, Kulak SC, Kozlowski K, Obeidat M, Jahroudi N, Paes J, Berryman M, Ballermann BJ. CLIC5A, a component of the ezrin-podocalyxin complex in glomeruli, is a determinant of podocyte integrity. Am J Physiol Renal Physiol. 2010; 298:F1492–F503. [PubMed: 20335315]

Zhang DS, Piazza V, Perrin BJ, Rzadzinska AK, Poczatek JC, Wang M, Prosser HM, Ervasti JM, Corey DP, Lechene CP. Multiisotope imaging mass spectrometry reveals slow protein turnover in hair-cell stereocilia. Nature. 2012; 481:520–524. [PubMed: 22246323]

Zhao H, Williams DE, Shin JB, Brugger B, Gillespie PG. Large membrane domains in hair bundles specify spatially constricted radixin activation. J Neurosci. 2012; 32:4600–4609. [PubMed: 22457506]

Zheng L, Sekerkova G, Vranich K, Tilney LG, Mugnaini E, Bartles JR. The deaf jerker mouse has a mutation in the gene encoding the espin actin-bundling proteins of hair cell stereocilia and lacks espins. Cell. 2000; 102:377–385. [PubMed: 10975527]

Zheng L, Zheng J, Whitlon DS, Garcia-Anoveros J, Bartles JR. Targeting of the hair cell proteins cadherin 23, harmonin, myosin XVa, espin, and prestin in an epithelial cell model. J Neurosci. 2010; 30:7187–7201. [PubMed: 20505086]

Zuo J. Transgenic and gene targeting studies of hair cell function in mouse inner ear. J Neurobiol. 2002; 53:286–305. [PubMed: 12382282]

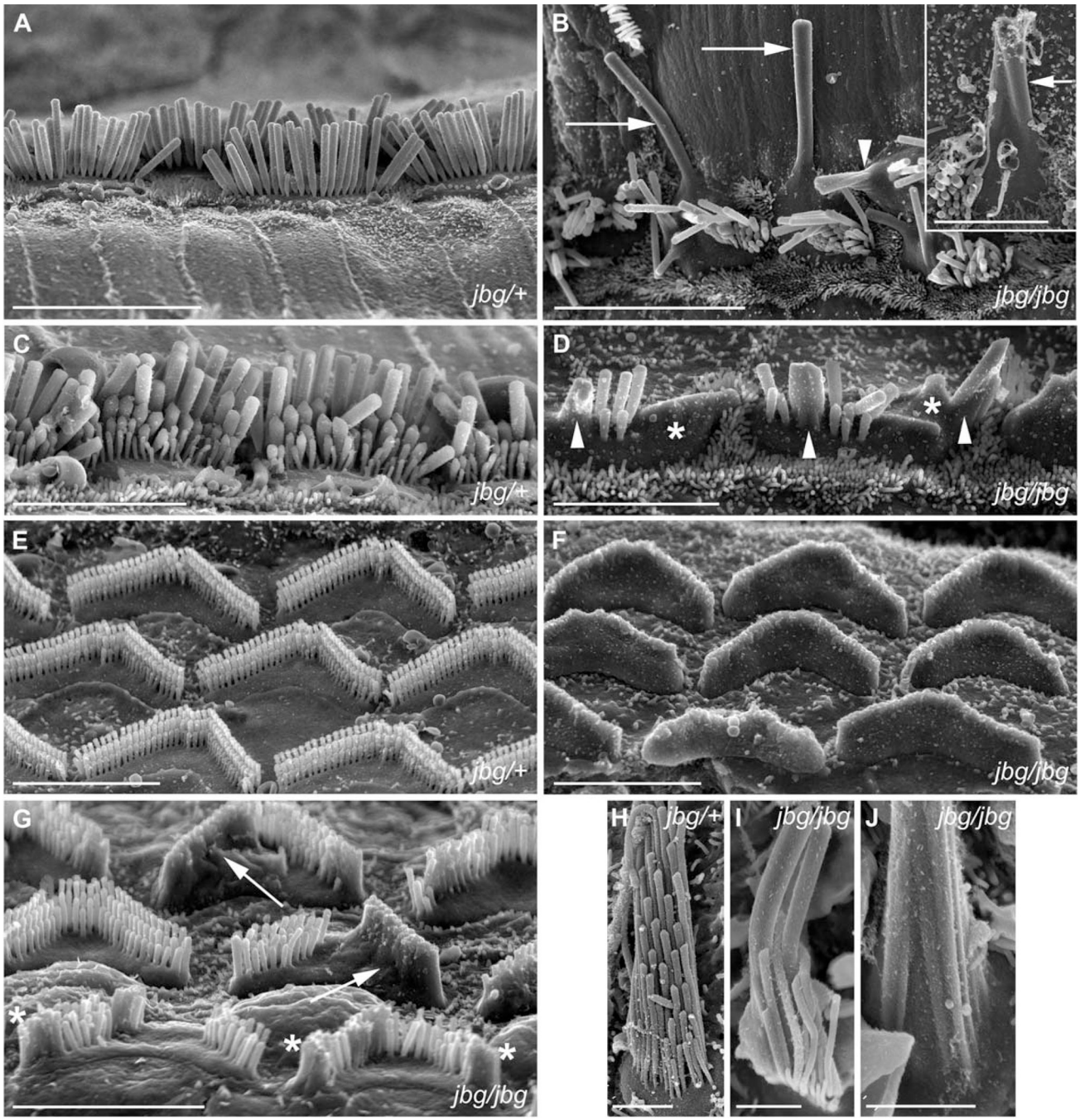


**Fig. 1.**

Morphological defects of hair cells in *jitterbug* mutant. Auditory (A–G) and vestibular (H–J) hair cells from P17 and P10 (inset) mice. (**A**) Inner hair cells (IHC) from a heterozygous control (*jbg*/+) viewed from lateral aspect near the apex of the cochlear duct. (**B**) IHC near the apex of a cochlea from a *jitterbug* mutant (*jbg/jbg*) showing elongated and fused stereocilia lying parallel to the surface of the epithelium (arrows), and fused stereocilia with lifted membranes (arrowhead). Inset shows IHC with fused stereocilia (arrow) at P10. (**C**) Control IHC at the base with staircase arrangement of stereocilia. (**D**) Mutant IHC at the

base lack the shortest row of stereocilia and exhibit fusion of several stereocilia (arrowheads) as well as mass fusion indicated by the lifted plasma membrane (*). (**E**) Outer hair cells (OHC) at the base of control cochlear duct showing regular arrangement of stereocilia arrays. (**F**) OHC at the base of a mutant cochlear duct devoid of individual, non-fused stereocilia. (**G**) OHC from mid-turn of mutant cochlear duct with varying degrees of stereocilia fusion, including entire arm of V-shaped bundle (arrows) and fusion at the ends of bundles (*). (**H**) Utricular hair cells (UHC) from heterozygous control showing stereocilia arranged in rows of increasing height and uniform diameter within each row. (**I**) Mutant UHC bundle lacks a regular staircase array and displays thickened stereocilia. (**J**) High magnification view of proximal end of mutant UHC bundle with a morphology reflecting apparent fusion of multiple parallel actin bundles covered by a common membrane. Scale bars: 10 μm (A, B), 5 μm (inset, C, D, E, F, G), 2 μm (H–J).

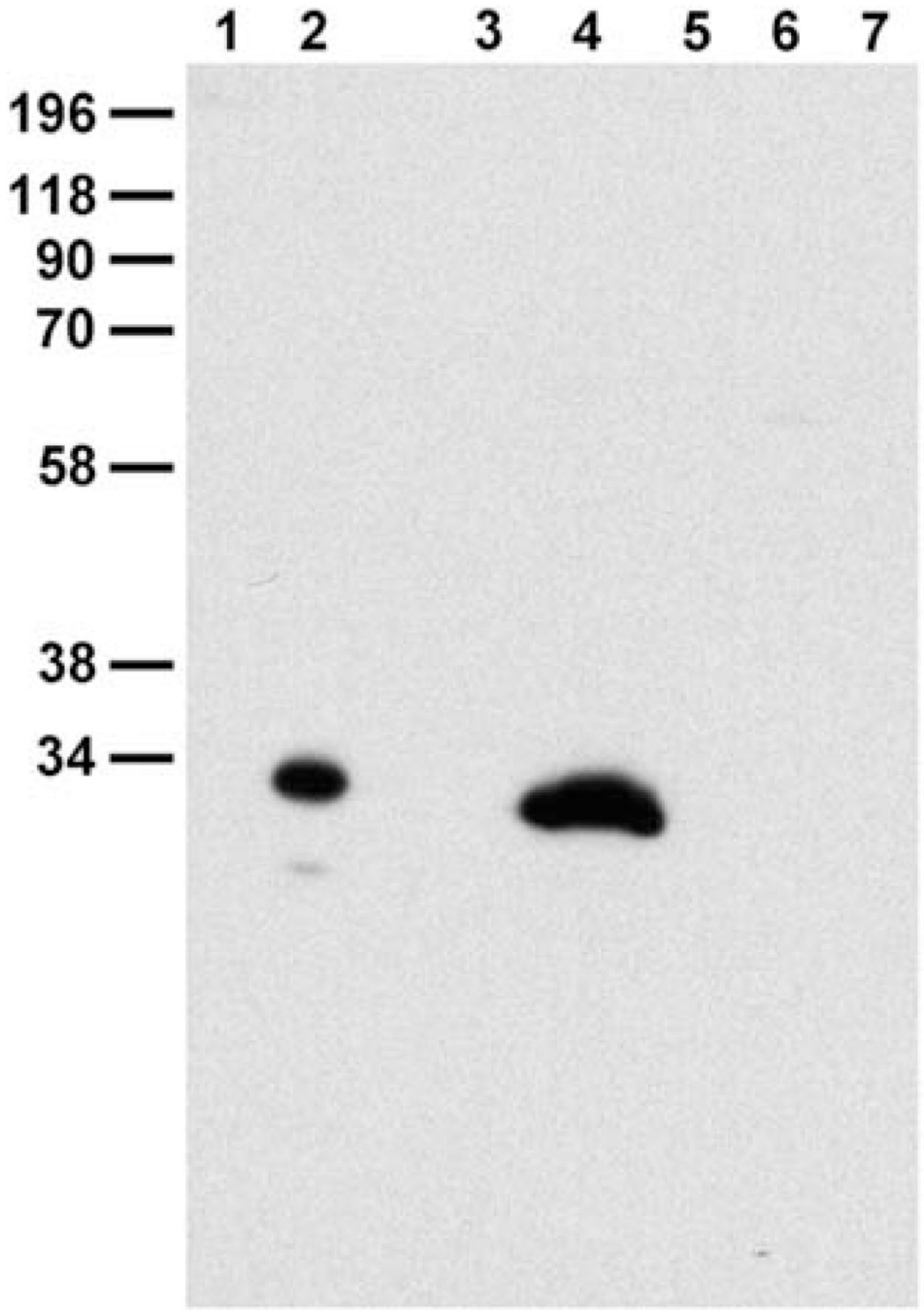


**Fig. 2.**

Characterization of monospecific CLIC5 antibody (APB56) on Western blot. Blot probed with CLIC5 polyclonal antibody following cross-adsorption against CLIC4 and subsequent affinity-purification on CLIC5 (APB56). (Lanes 1, 2), bacterial extract containing 50 ng untagged recombinant CLIC4 and CLIC5, respectively; (Lanes 3–7), 10 mg SDS-soluble extract of mouse stomach, lung, pancreas, small intestine, and liver, respectively. APB56 does not cross-react with CLIC4; a single major band is detected in lung extract.

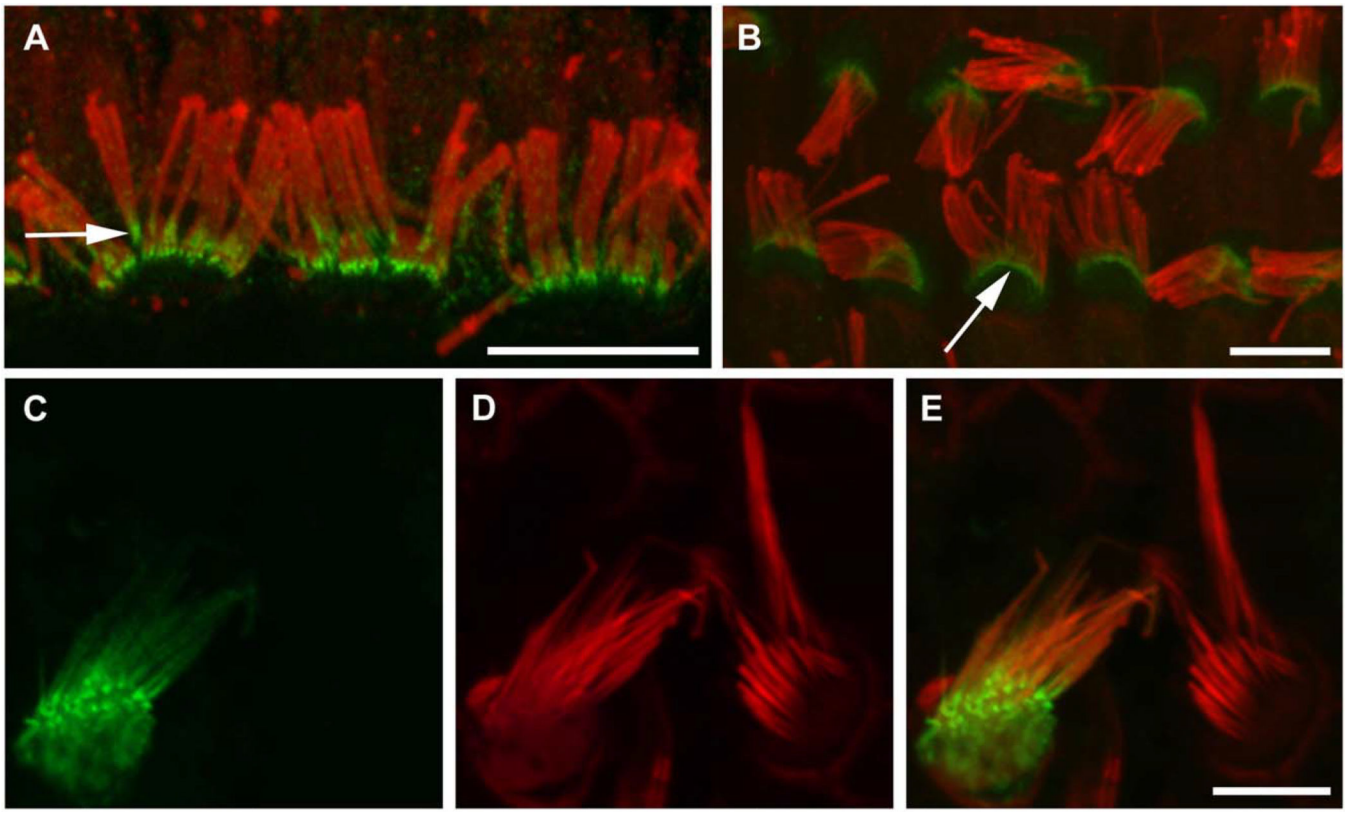


**Fig. 3.**

CLIC5 concentrates at the base of the hair bundle. (**A, B**) Fluorescence confocal micrographs of adult rat whole mount organ of Corti preparations stained with specific antibody (APB56) against CLIC5 (green); actin filaments were counterstained with phalloidin (red). Specimens were gently squashed to facilitate visualization of staining along the proximal-distal axis of stereocilia; note that requisite use of heat-induced antigen retrieval compromised the morphological preservation of bundles as well as the quality of F-actin staining. In both inner (A) and outer (B) hair cells, CLIC5 is concentrated at the base of stereocilia (arrows). (**C–E**) Expression of GFP-CLIC5 fusion protein in vestibular hair cell. The transfected cell (C) exhibits accumulation of CLIC5 towards the proximal end of the stereocilia. (D) Actin filaments were counterstained with phalloidin (red). (E) Merged images of C and D. Scale bars: 5 μm. [Color figure can be viewed in the online issue, which is available at wileyonlinelibrary.com.]

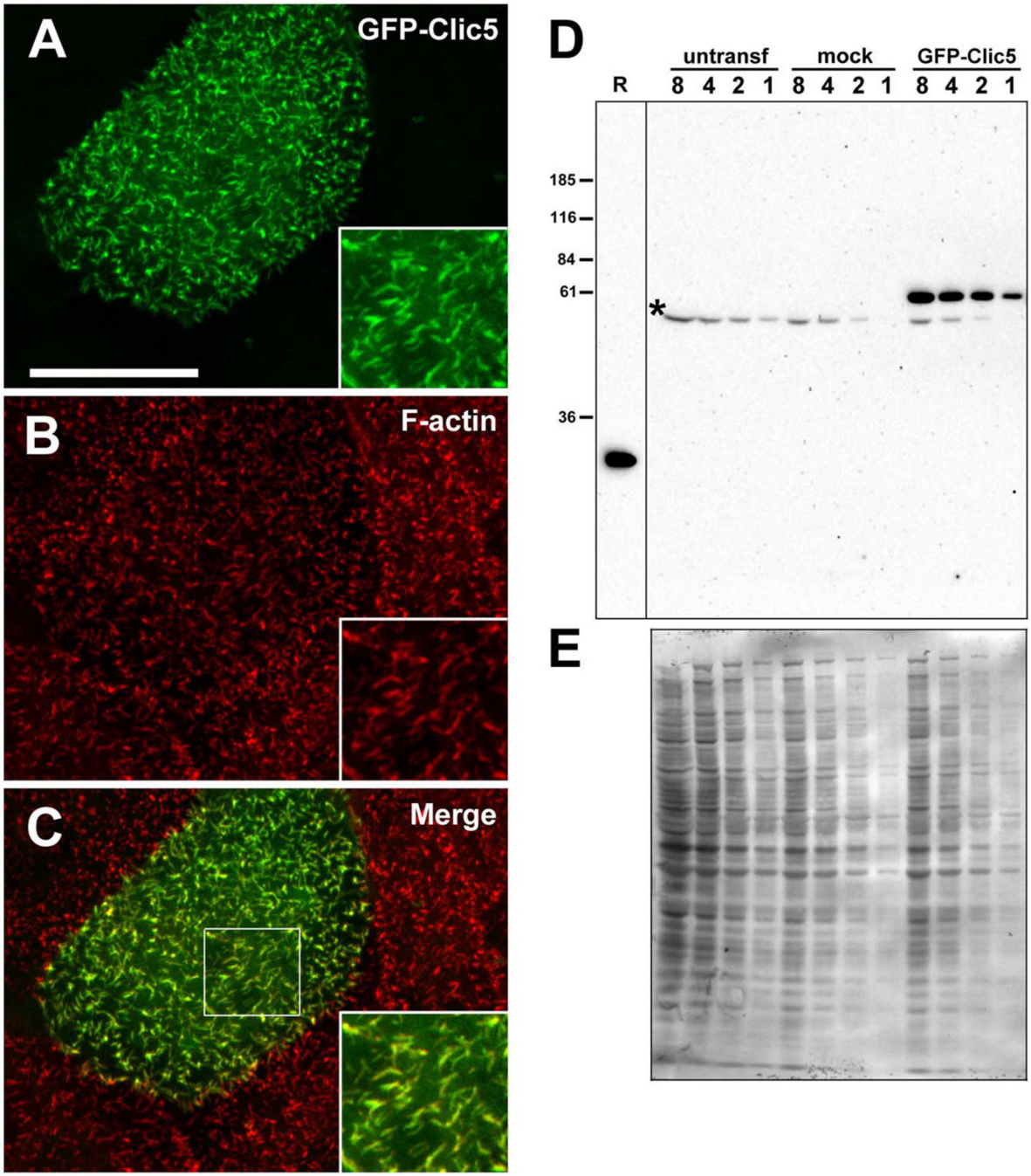


**Fig. 4.**

Characterization of GFP-CLIC5 fusion protein. (A–C) LLC-PK1-CL4 epithelial cell transfected with GFP-CLIC5 (**A**) and counterstained with phalloidin (**B**). Merged images (**C**) with boxed area to indicate region shown in insets. GFP-CLIC5 concentrates in microvilli-like surface structures rich in F-actin. Scale bar: 20 μm. (**D**) Western blot of LLC-PK1-CL4 extracts probed with whole antiserum (B132) against CLIC5. Blot contains two-fold serial dilutions (lanes 8, 4, 2, 1) of extracts from untransfected (untransf), mock-transfected cells treated with transfection reagent with no DNA and GFP-CLIC5 transfected

cultures. Bacterial lysate containing 50 ng untagged human CLIC5 (R) was loaded on the same gel as a positive control. A band migrating between ~55 and 60 kDa and corresponding to the expected size of the fusion protein is detected only in the GFP-CLIC5 culture; a faster migrating background band (*) is seen in all cultures. Note that no endogenous CLIC5 (~32 kDa) was detected. (**E**) Western blot stained with Coomassie Blue as a loading control. [Color figure can be viewed in the online issue, which is available at wileyonlinelibrary.com.]

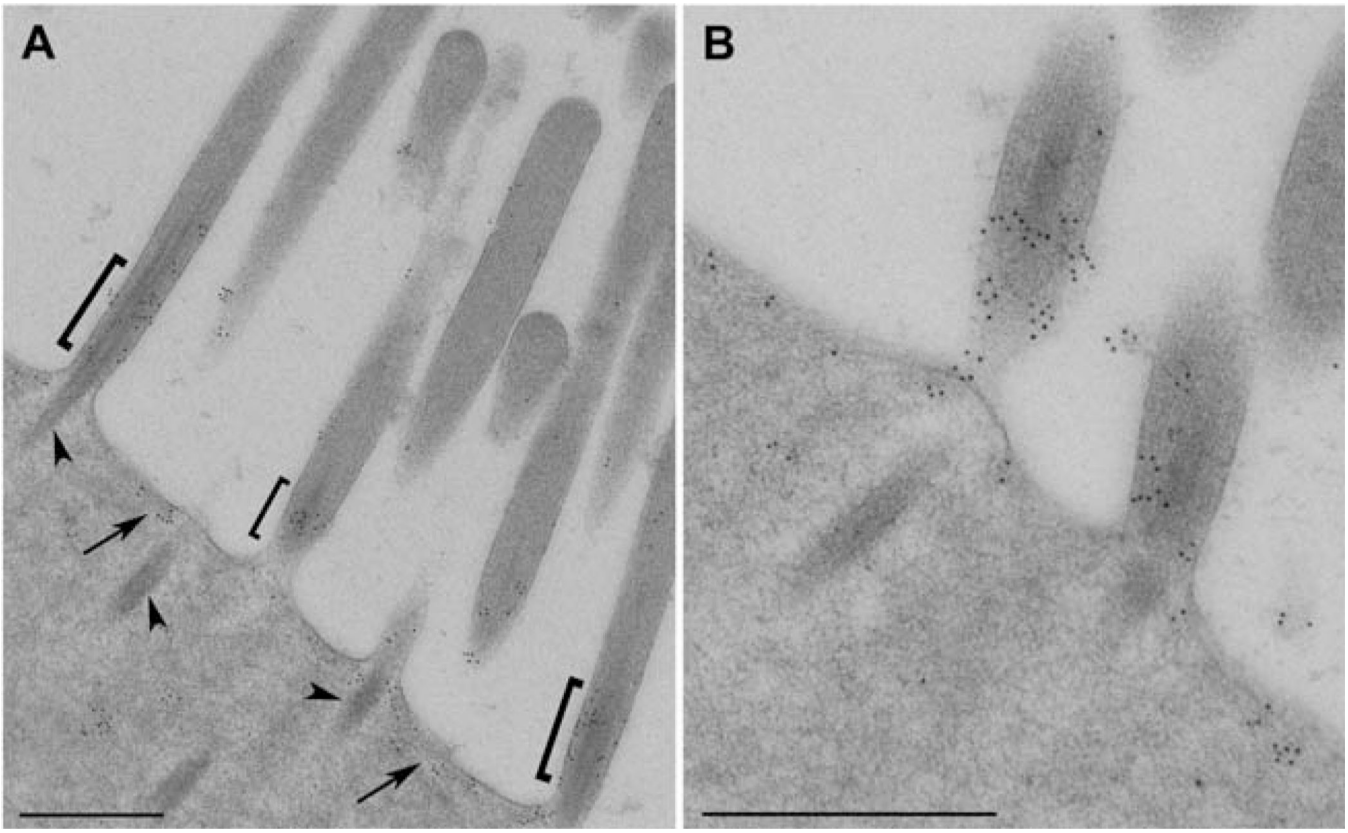


**Fig. 5.**

Immunogold localization of CLIC5 at the apical surface of inner hair cells from adult rat. (**A**) Low magnification overview showing high density of gold particles at the bases of stereocilia (brackets) as well as the inter-stereocilia membrane domain (arrows); gold labeling is sparse at the tips and shafts of stereocilia as well as core actin rootlets projecting into the cutic-ular plate (arrowheads). (**B**) High magnification of CLIC5 staining at the base of stereocilia and inter-stereocilia region. Scale bars: 500 nm.

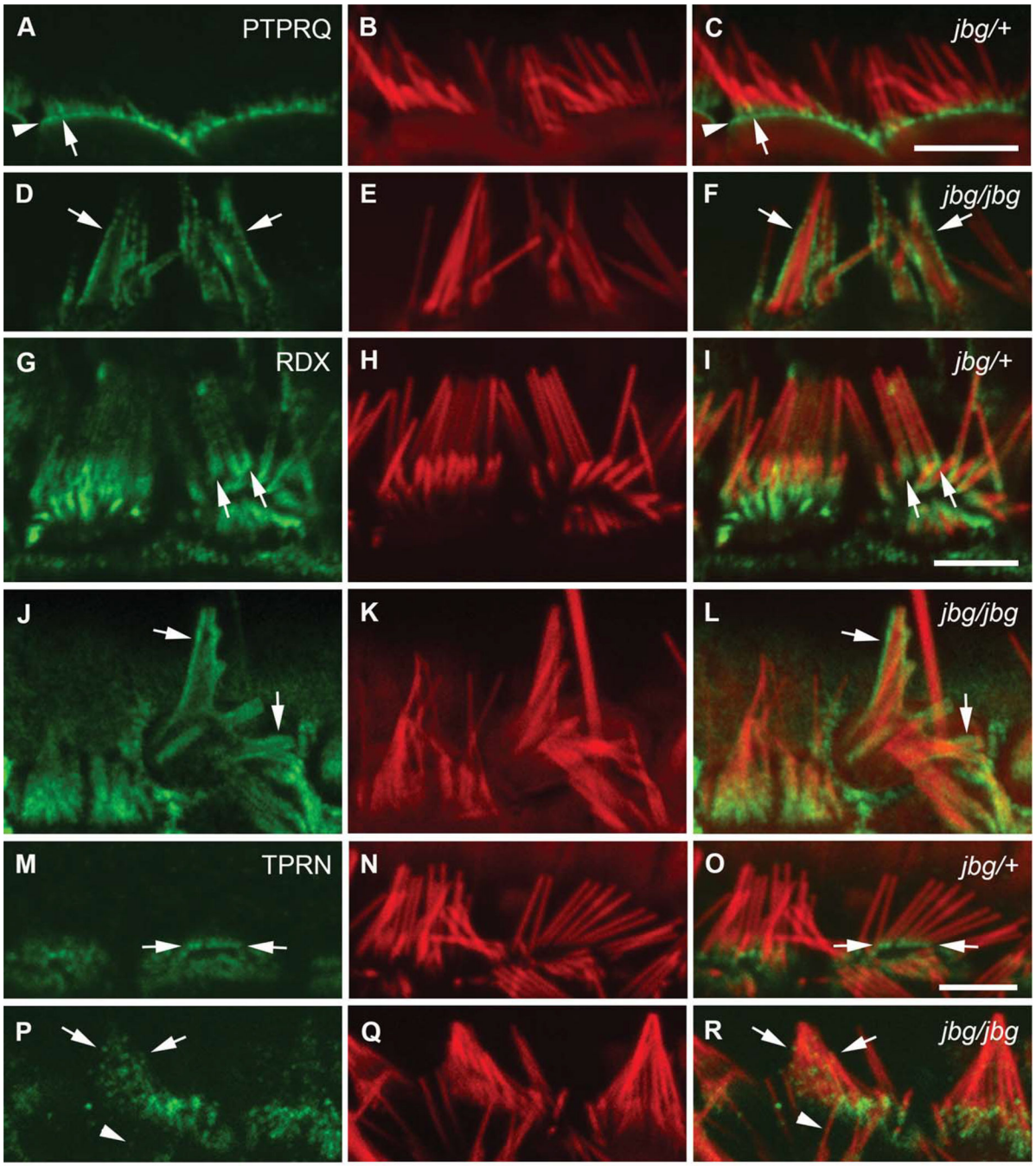


**Fig. 6.**

Localization of PTPRQ, RDX, and TPRN in mature hair cells of *jitterbug* mutant. Inner hair cells near the apex of the cochlea stained with antibodies (green) against PTPRQ at P40 (**A–F**), RDX at P17 (**G–L**), and TPRN at P21 (**M–R**) and counterstained with phalloidin (red). (**A-F**) In control cells (*jbg*/+), intense PTPRQ staining is restricted to the bases of stereocilia (A, C, arrow) as well as the intervening apical plasma membrane (A, C, arrowhead); in mutant cells (*jbg/jbg*), PTPRQ is distributed in a diffused pattern extending along the membrane covering the shaft of the still recognizable stereocilia (D, F, arrows). (**G-L**)

Control cells exhibit enriched RDX staining at the base and a lower level of staining along the stereocilia shaft towards the tip (G, I, arrows); mutant cells exhibit a diffuse pattern of RDX staining extending along the membrane covering the shaft of the still recognizable, but severely malformed stereocilia (J, L, arrows). (**M–R**) In control cells, TPRN staining is enriched at the base of stereocilia (M, O, arrows); in mutant cells, TPRN staining is distributed in a diffused pattern extending along the shaft of the malformed stereocilia (P, R, arrows). TPRN staining is also dispersed along the shaft of a single individual stereocilium (P, R, arrowhead). Scale bars: 5 μm.

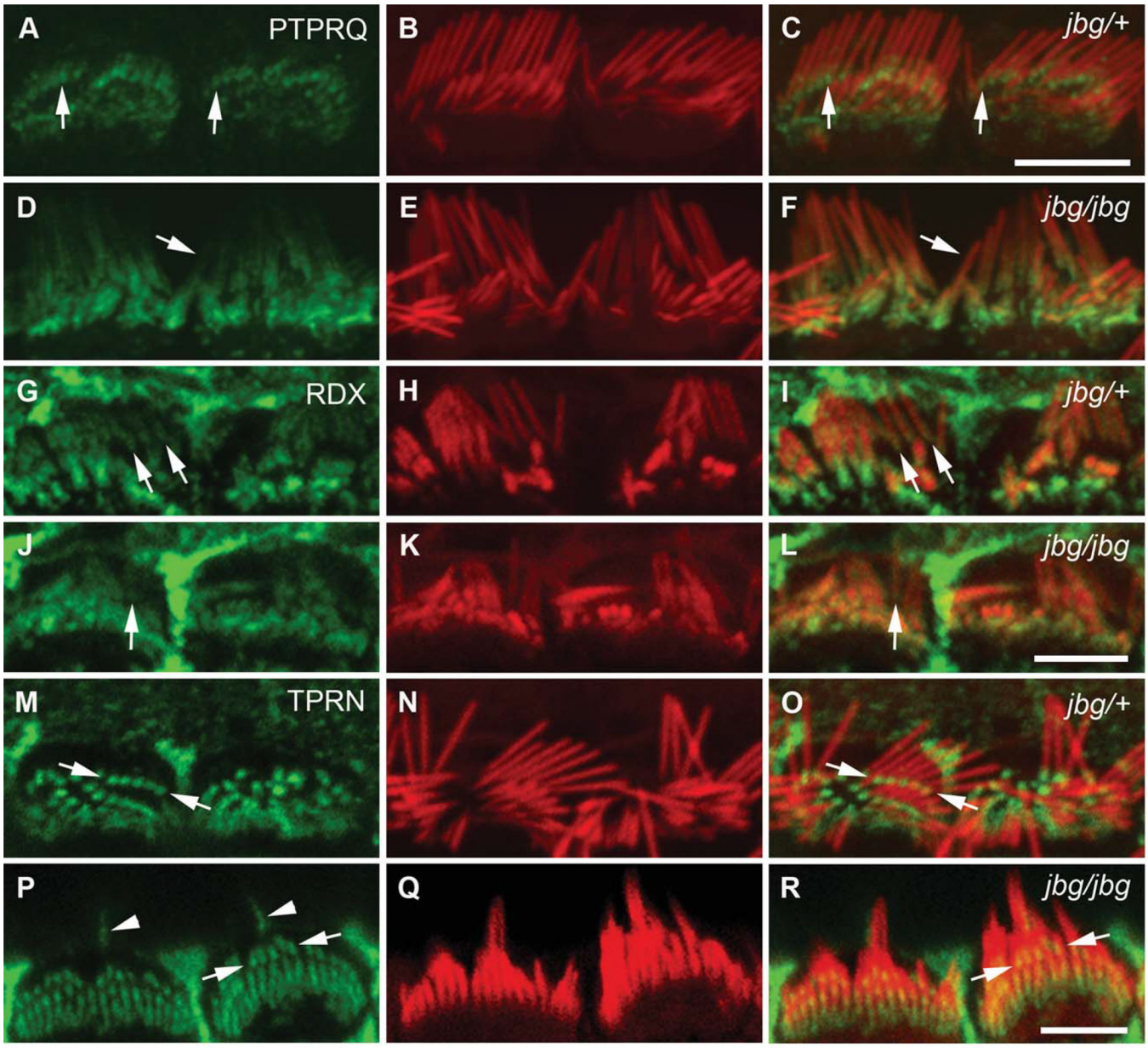


**Fig. 7.**

Localization of PTPRQ, RDX, and TPRN in immature hair cells of *jitterbug* mutant. Inner hair cells near the apex of the cochlea stained with antibodies (green) against PTPRQ at P10 (**A–F**), RDX at P7 (**G–L**), and TPRN at P10 (**M–R**) and counter-stained with phalloidin (red). (**A–F**) In control cells (*jbg*/+), PTPRQ is enriched at the bases of stereocilia (A, C, arrows); in mutant cells (*jbg/jbg*), PTPRQ labeling extends along the stereocilia shaft and is not restricted to the base (D, F, arrow). (**G–L**) Control cells exhibit RDX staining enriched at the bases of stereocilia (G, I, arrows); in mutant cells a small amount of RDX extends along the shaft towards the tip of a single stereocilium (J, L, arrow). (**M–R**) TPRN staining is restricted to the bases of stereocilia in control cells (M, O, arrows) as well as mutant cells

(P, R, arrows). Kinocilia are stained positive with the TPRN antibody (P, R, arrowheads). Scale bars: 5 μm.

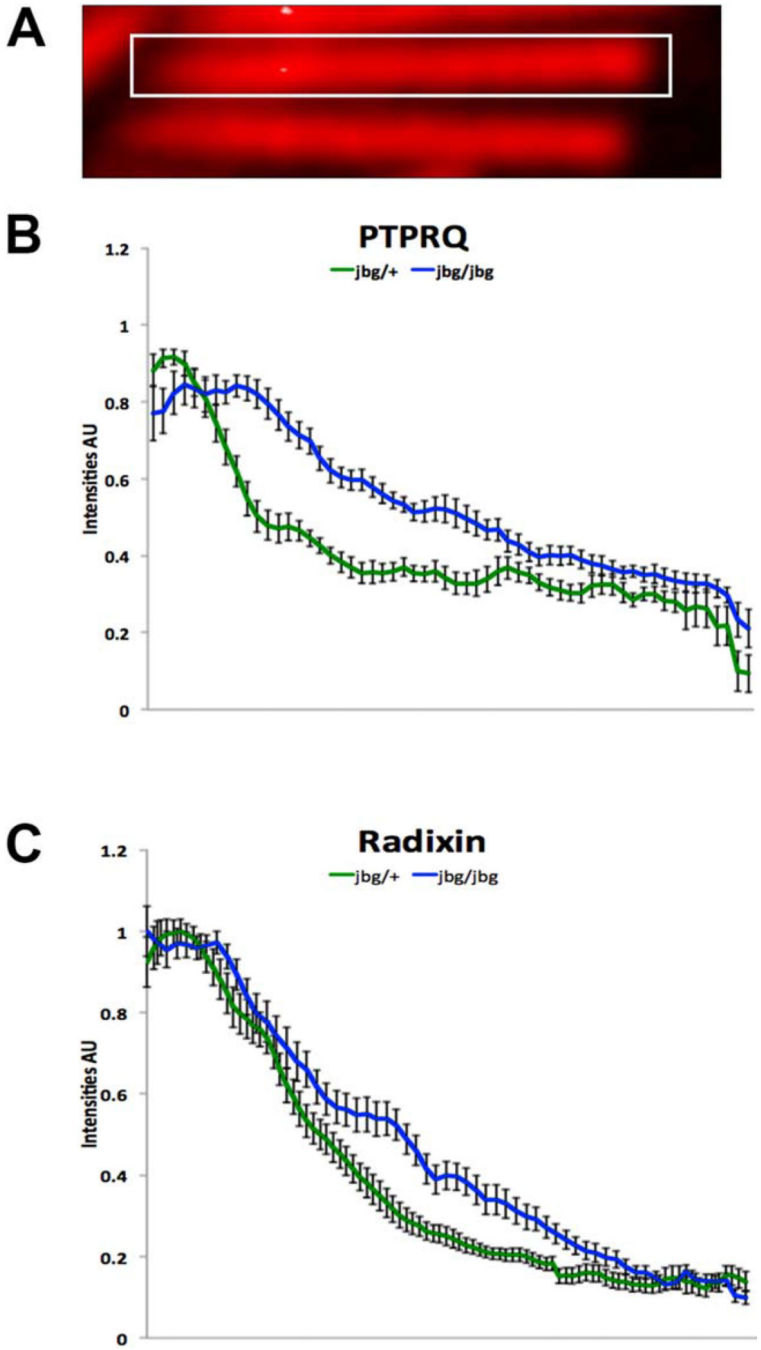


**Fig. 8.**

PTPRQ and RDX redistribute along the lengths of stereocilia at P10 in *jitterbug* mutant mice. Analysis of PTPRQ (B) and RDX (C) distributions in control (*jbg*/+) and mutant (*jbg/jbg*) stereocilia. (**A**) For measurement, a rectangular selection was drawn along the length of stereocilia from base (left) to tip (right), and intensity profiles obtained in ImageJ (NIH). Plots show mean intensities (AU, arbitrary units) ± S.D. (*n* = 10 stereocilia from the tallest row of inner hair cells). In control stereocilia, PTPRQ is very concentrated at the base with relatively low expression towards the tips (**B**, lower green line), similar to the distribution of

RDX (**C**, lower green line). In mutant stereocilia, the proteins show an altered distribution, no longer as restricted to a high expression at the base and with redistribution along the shaft (**B and C**, upper blue lines). [Color figure can be viewed in the online issue, which is available at wileyonlinelibrary.com.]

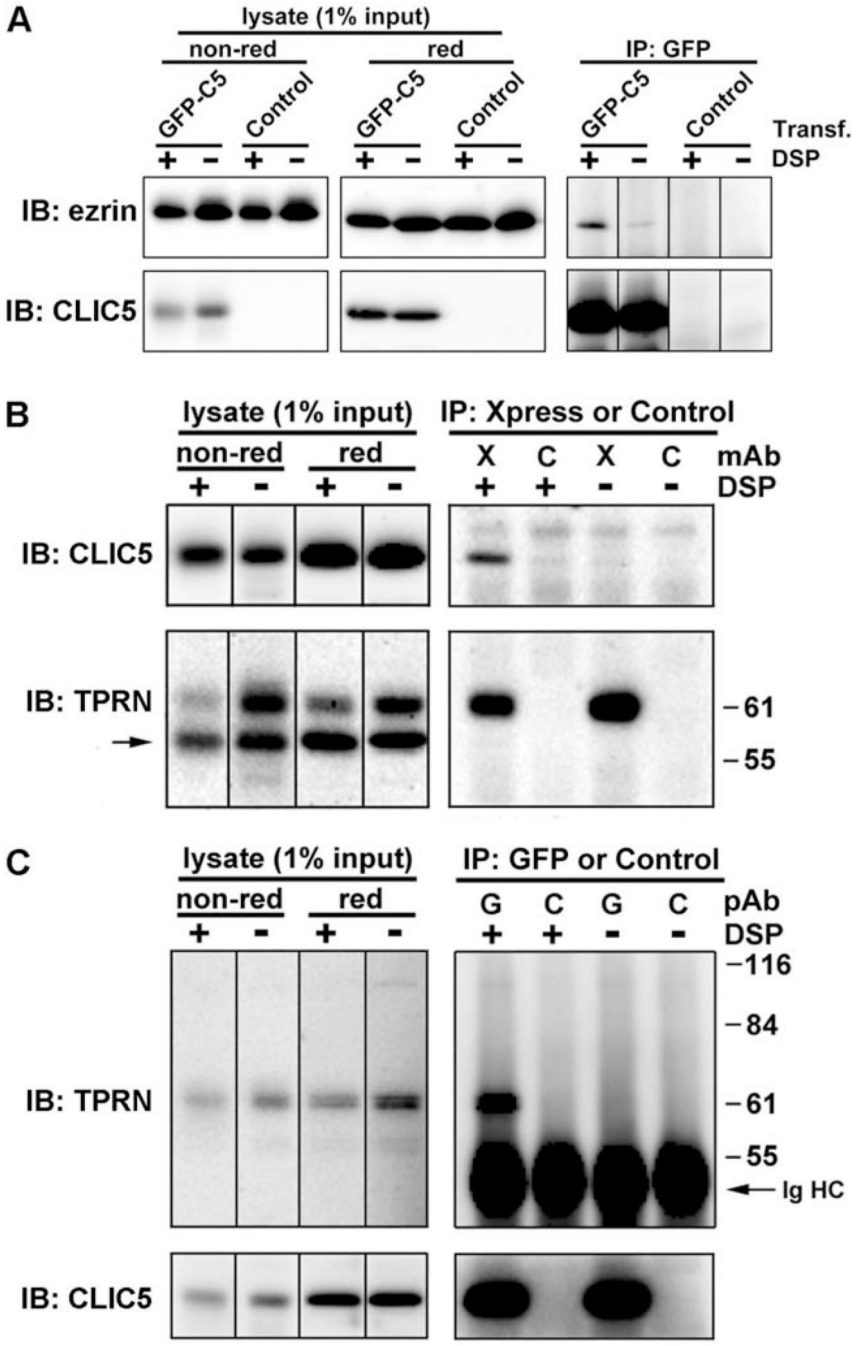


**Fig. 9.**

CLIC5 associates with Ezrin and TPRN in LLC-PK1 epithelial cells. (**A**) Endogenous ezrin coimmunoprecipitates with GFP-CLIC5. Cells transfected with GFP-CLIC5 (GFP-C5) or mock-transfected (Control) were treated with DSP (+) or DMSO alone (−), followed by immunoprecipitation with GFP antibody. Immunoblots of starting lysates (nonreduced and reduced) and immunoprecipitates were probed with ezrin polyclonal antibody and then reprobed with CLIC5 polyclonal antibody. (**B**) GFP-CLIC5 coimmunoprecipitates with the C-terminal region of TPRN. Cells double transfected with GFP-CLIC5 and Xpress-

TPRN$^{308–711}$ were treated with DSP (+) or DMSO alone (−), followed by immunoprecipitation with antibody against the Xpress epitope (X) or an isotype matched control (C) monoclonal antibody. Immunoblots were probed with CLIC5 polyclonal antibody and then reprobed with TPRN polyclonal antibody (TPRN); band indicated by the arrow corresponds to CLIC5. (**C**) Xpress-TPRN$^{308–711}$ coimmunoprecipitates with GFP-CLIC5. Double transfected cells were treated with DSP (+) or DMSO (−) followed by immunoprecipitation with antibodies against GFP (G) or a control (C) polyclonal antibody. Immunoblots were probed with TPRN polyclonal antibody and then reprobed with whole antiserum against CLIC5. IgG heavy chain (Ig HC) is indicated.

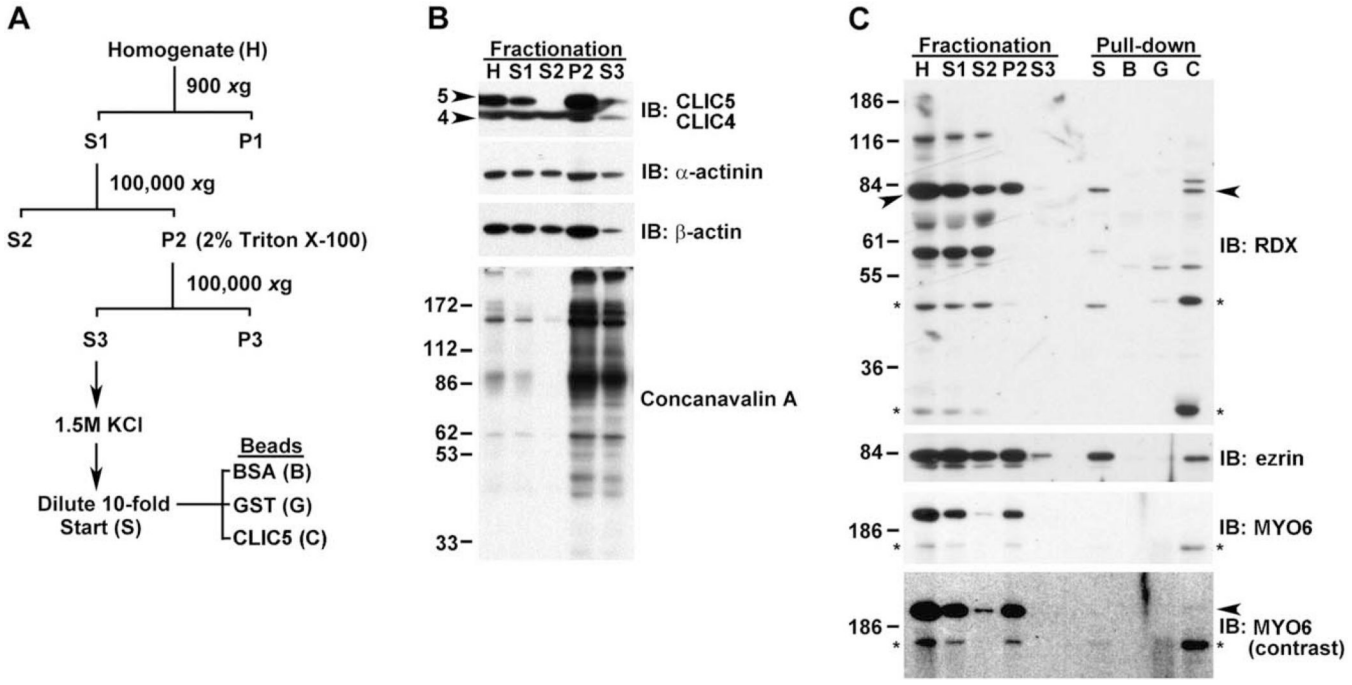


**Fig. 10.**

CLIC5 associates tightly with the detergent-insoluble actin cytoskeleton and interacts with RDX, ezrin, and MYO6 in an affinity pull-down assay using mouse lung extract. (**A**) Summary of scheme used to fractionate lung tissue. (**B**) Blots containing fractions were probed with antibodies that recognize both CLIC5 (arrowhead, 5) and CLIC4 (arrowhead, 4), antibodies against α-actinin and β-actin, and the lectin concanavalin A to detect glycosylated membrane proteins. Equal volumes were loaded for H, S1, and S2; 10 times more sample was loaded for P2 and S3. CLIC5 was highly insoluble and resistant to extraction with detergent (S3), indicating a tight association with the cytoskeleton; α-actinin and β-actin, both of which are cytoskeletal proteins, show relatively poor recovery after detergent treatment in comparison to glycosylated membrane proteins detected by concanavalin A (compare P2 and S3). (**C**) Blots containing equivalent volumes of fractions as well as starting material (S) and eluates from BSA (B), GST (G), or 6His-CLIC5 (C) beads used in the pull-down assay. RDX antibody detects a major band migrating at ~82 kDa (arrowheads) and several additional faster migrating bands that may represent RDX degradation products; RDX is highly resistant to detergent extraction (compare P2 and S3). In the pull-down assay, RDX is present only in the CLIC5 bead eluate (arrowhead). Two potential degradation products (*) are enriched in the CLIC5 eluate relative to the starting extract or fractionation samples, suggesting that these fragments have greater affinity for CLIC5 than intact RDX. Ezrin antibody recognizes a major band at ~82 kDa. In the pull-down assay, ezrin is detected only in the CLIC5 eluate. MYO6 antibody recognizes a prominent band migrating at ~200 kDa and a faster migrating band at ~160 kDa (*); MYO6 is highly resistant to detergent extraction (compare P2 and S3). The similar fractionation profiles of the prominent and faster migrating band (*) suggests that the latter is a MYO6 degradation product. The faster migrating species is enriched in the CLIC5 eluant. With

increased contrast, a faint band (arrowhead) corresponding to the ~200 kDa migrating intact MYO6 band is detected in the CLIC5 eluate.

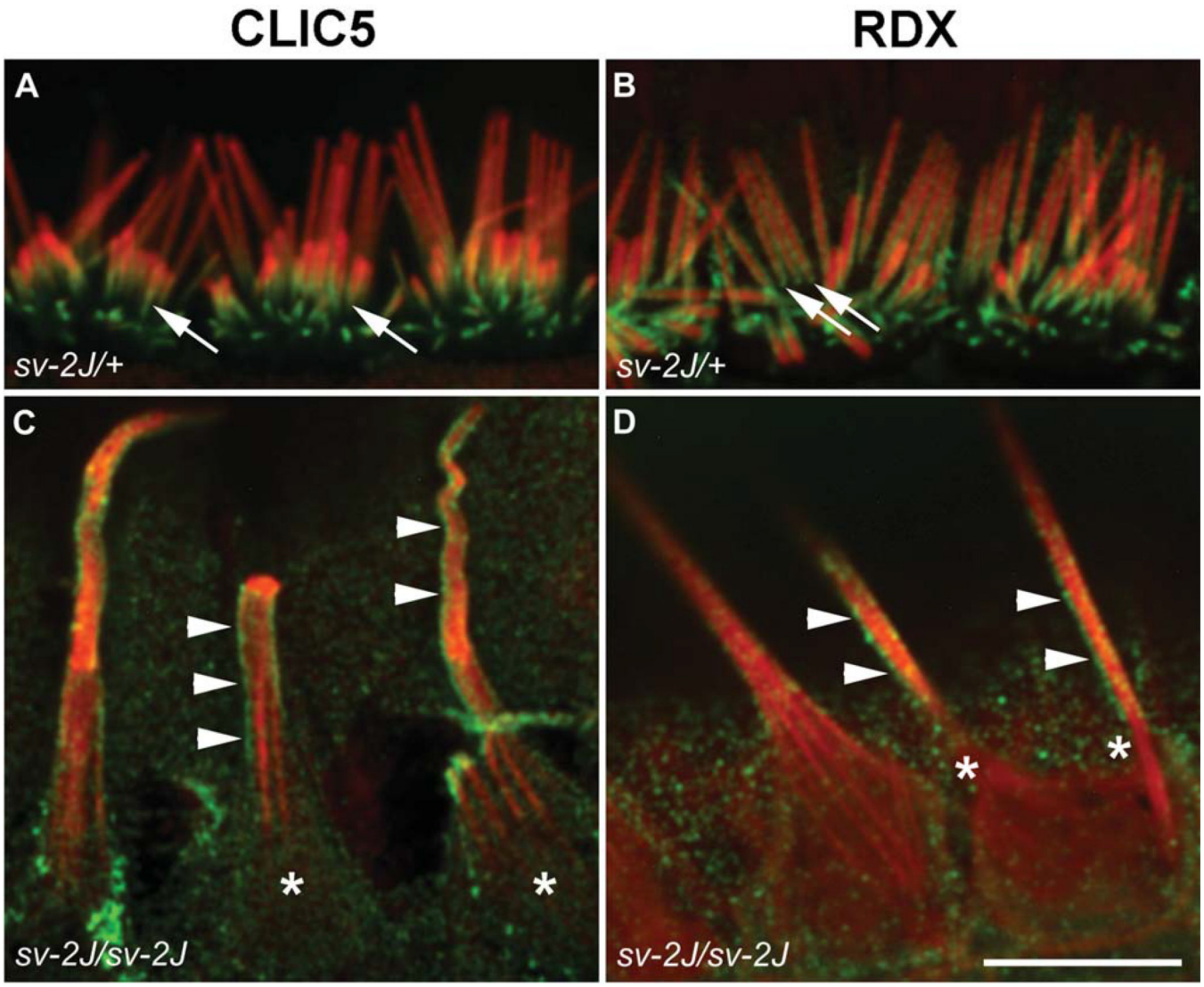


**Fig. 11.**

Localization of CLIC5 and RDX in hair cells from *Myo6* mutant Snell's waltzer 2 Jackson (*sv-2J*) mice. Inner hair cells from the apex of P15 cochleae from heterozygous control (*sv-2J*/+) mice (**A, B**) and homozygous mutant (*sv-2J/sv-2J*) mice (**C, D**). Hair cells were stained with antibodies (green) against CLIC5 (A, C) or RDX (B, D) and counterstained with phalloidin (red). Both proteins are enriched at the base of stereocilia in control cells (arrows). However, in *Myo6* mutant cells, both proteins exhibit diffused staining along the shaft of giant fused stereocilia. Staining of CLIC5 and RDX is enriched at the surface of shafts (arrowheads), indicating preferential association with the membrane; accumulation of CLIC5 or RDX is no longer seen at the bases of fused stereocilia (asterisks). Scale bar: 10 μm.

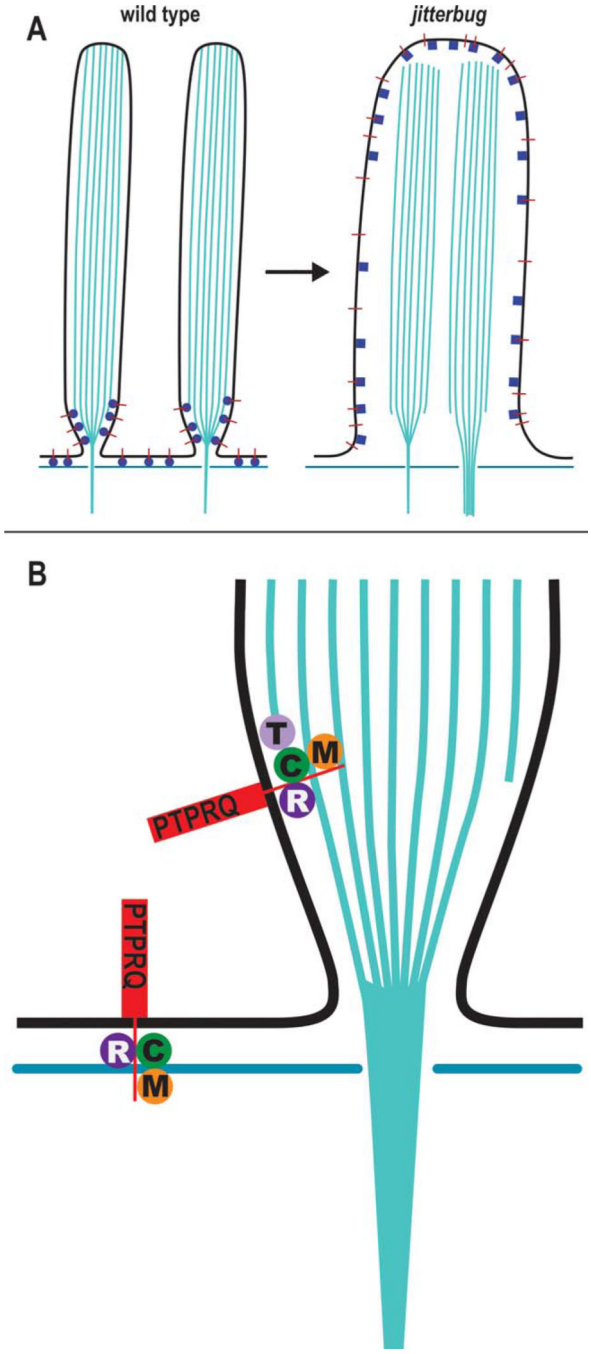


**Fig. 12.**

Simplified model for membrane-cytoskeletal linking complex at the base of stereocilia. (**A**) In stereocilia of wild-type hair cell (left panel) the cytoplasmic domain of PTPRQ (red lines) associates with a juxtamembrane protein complex (blue spheres) consisting of CLIC5, RDX, MYO6, and/or TPRN, thereby linking PTPRQ to actin filaments at the tapered base of stereocilia as well as linking actin filaments of the cuticular plate with the interstereocilia membrane domain. In the absence of CLIC5 (right panel), the protein complex is altered (blue squares), thereby compromising function and possibly dissociation of interacting

partners, leading to destabilized membrane-cytoskeletal attachments, consequent membrane lifting, and loss of stereocilia individuality. (**B**) Hypothetical molecular complexes linking PTPRQ to submembranous actin: CLIC5 (C), RDX (R), MYO6 (M), and TPRN (T). Based on homology with the minus end-capping protein phostensin [Lai et al., 2009; Rehman et al., 2010; Wang et al., 2012], TPRN may associate with the minus ends of actin filaments that may terminate at the tapered base. MYO6 minus-end directed motor activity could help establish and dynamically maintain the localization of the protein complex at the base of stereocilia and simultaneously act on its own as an independent membrane-cytoskeletal linker. [Color figure can be viewed in the online issue, which is available at wileyonlinelibrary.com.]